Published in final edited form as:

Small. 2024 February ; 20(7): e2305426. doi:10.1002/smll.202305426.

Nanomaterial-Enabled Photothermal Heating and Its Use for Cancer Therapy *via* Localized Hyperthermia

Song Shen,

The Wallace H. Coulter Department of Biomedical Engineering, Georgia Institute of Technology and Emory University, Atlanta, Georgia 30332, USA

College of Pharmaceutical Sciences, Jiangsu University, Zhenjiang, Jiangsu 212013, China

Qiu Jichuan,

The Wallace H. Coulter Department of Biomedical Engineering, Georgia Institute of Technology and Emory University, Atlanta, Georgia 30332, USA

Huo Da,

The Wallace H. Coulter Department of Biomedical Engineering, Georgia Institute of Technology and Emory University, Atlanta, Georgia 30332, USA

Younan Xia

The Wallace H. Coulter Department of Biomedical Engineering, Georgia Institute of Technology and Emory University, Atlanta, Georgia 30332, USA

School of Chemistry and Biochemistry, Georgia Institute of Technology, Atlanta, Georgia 30332, USA

Abstract

Photothermal therapy (PTT), which employs nanoscale transducers delivered into a tumor to locally generate heat upon irradiation with near-infrared light, shows great potential in killing cancer cells through hyperthermia. The efficacy of such a treatment is determined by a number of factors, including the amount, distribution, and dissipation of the generated heat, as well as the type of cancer cell involved. The amount of heat generated is largely controlled by the number of transducers accumulated inside the tumor, the absorption coefficient and photothermal conversion efficiency of the transducer, and the irradiance of the light. The efficacy of treatment depends on the distribution of the transducers in the tumor and the penetration depth of the light. The vascularity and tissue thermal conduction both affect the dissipation of heat and thereby the distribution of temperature. The successful implementation of PTT in the clinic setting critically depends on techniques for real-time monitoring and management of temperature.

Graphical Abstract

Photothermal therapy demonstrates great potential in killing cancer cells through hyperthermia. The effect is affected by lots of parameters, such as the laser, photothermal transducers, spatial

---

younan.xia@bme.gatech.edu .

distribution of the transducers, bio-effect of the tissue (heat-sink effect, thermal conductivity), real-time monitoring of the temperature.

Keywords

photothermal therapy; gold nanoparticles; hyperthermia; thermotolerance; temperature monitoring

1. Introduction

Hyperthermia refers to an acute condition that occurs when the body produces more heat than it can be dissipated. Clinically, hyperthermia can be created artificially using drugs and/or medical devices and leveraged for cancer treatment.[1,2] If the temperature surges to 42 °C and above, it will cause many proteins in the cell to irreversibly denature and thus induce apoptosis. In addition, the elevated temperature can enhance chemotherapy, offering an opportunity to reduce the amount of the therapeutic agent without compromising its efficacy toward a treatment.[3] In the past, the generation of heat typically involves the use of external electromagnetic waves with wavelengths in the radiofrequency, ultrasound, or microwave region.[4–6] These methods often lack selectivity and have significant side effects as a result of severe damage to the normal tissues surrounding a tumor. Recently, localized hyperthermia enabled by the magnetic nanoparticles delivered into a tumor has received considerable attention owing to its potential for localized, target-specific heating.[7] In principle, such a technique can be applied to exclusively heat the tumor by means of energy loss from the magnetic nanoparticles placed in an external alternating magnetic field, helping improve the selectivity and efficacy of a treatment.

Parallel to the magnetic means, localized hyperthermia based on photothermal conversion has also gained major attention in recent years.[8–11] The component key to this approach is a photothermal transducer or agent (typically, in the form of nanoparticle) that can absorb light and then convert the absorbed photons to phonons (*i.e.*, heat) with high efficiency. In such a treatment (Figure 1), known as photothermal therapy (PTT), each transducer acts as an individual heating unit, offering an opportunity to realize localized hyperthermia with high spatial resolution. When conjugated with an antibody or other targeting ligands, the transducer can be equipped with the ability to selectively target a cancer cell by binding to the specific receptor overexpressed on the membrane.[12,13] By controlling the irradiance and/or duration of the light, this approach offers a highly selective means for cancer treatment, with damage to the exposed healthy tissues being potentially minimized to a negligible level. One of the technical requirements for *in vivo* applications is that the absorption peak of the transducer must be tuned into the near-infrared (NIR) region, including the 650–950 nm and 1000–1350 nm windows, in which the attenuation of light by blood and soft tissues is low enough to allow for deep penetration.[14,15]

Despite the successful implementation in a number of animal tumor models, the efficacy of PTT is still limited by a set of challenges (Figure 1), including the inadequate accumulation and often non-uniform distribution of the nanoscale transducers inside a solid tumor, the difference in heat dissipation between the central and peripheral regions, and the attenuation of light by the transducers themselves along the propagation path. In this review, we start with a brief introduction to the interactions between tissues and electromagnetic waves of different wavelengths, as well as the optical properties of various types of nanoscale transducers. We then discuss the biological barriers that affect the accumulation and distribution of nanoscale transducers in a solid tumor. Since the spatial-temporal profiles of temperature play a key role in a hyperthermia treatment, we also address technical issues related to heat dissipation, thermal conduction, as well as temperature monitoring during PTT.

2. Hyperthermia Therapy

During hyperthermia therapy, cells and tissues are exposed to elevated temperatures typically up to 10 degrees above the physiological temperature around 37 °C. The therapeutic effect of hyperthermia is mainly determined by the temperature, duration of heating, cancer type, and the ambient environment. In general, cancer cells are more sensitive to hyperthermia than normal cells because of their differences in extracellular microenvironment.[16,17] Due to the disorganized vascularity, the supplies of oxygen and nutrients cannot meet the demands of the growing tumor mass, resulting in the development of a hypoxic, acidic, and malnourished microenvironment.[18] Several studies have reported that cells under hypoxic and/or acidic conditions are more sensitive to the lethal effect from hyperthermia than cells in a normal environment.[19] Another reason for the increased thermo-sensitivity of tumor cells is the low capacity of heat dissipation. In healthy tissues, blood flow can increase dramatically with temperature in an effort to maintain the normal condition. The maximum flow capacity can be almost six times as high as the value prior to heating. In comparison, most solid tumors do not have this adaptive capacity due to their irregular vascularity and they can only double the maximum flow capacity when subjected to heating. As a result, the tumor is more quickly heated to the lethal temperature relative to healthy tissues.

Hyperthermia therapy will induce a variety of biological effects and these effects are usually temperature-dependent. Temperatures in the range of mild hyperthermia (39–41 °C) are non-lethal and can increase blood flow and metabolic rates, accelerating tissue healing. Mild hyperthermia will cause cell inactivation for several hours. However, heat shock responses will be initiated to combat the thermally-induced damage. This process includes the release of heat shock proteins, which will increase thermal resistance (known as thermotolerance) in the survival cells. The resistance is a temporary phenomenon, which can be overcome through prolonged heating.[20] Mild hyperthermia can improve antitumor immune responses, since it induces apoptosis and necrosis of cancer cells and produces enormous amounts of cell debris. The neoantigens in the debris stimulate the immune system and inhibit the growth of distal tumors, which is known as “abscopal effect”. However, the abscopal effect induced by hyperthermia is weak and insufficient for cancer inhibition. Combination with immunotherapy by blocking the immune checkpoint using the inhibitors of cytotoxic T-lymphocyte-associated protein 4 (CTLA-4),[21] indoleamine 2, 3-dioxygenase (IDO) [22,23] and programmed death-ligand 1 (PD-L1),[24, 25] is demonstrated to be a potential method to strengthen the therapeutic effect. There are also other possible mechanisms involving the hyperthermia-assistant immune responses, including the generation of heat shock proteins, regulation of immune cell proliferation, increased release of cytokines and tumor necrosis factor-alpha (TNF-α), as well as the promotion of lymphocyte trafficking.[26–28]

For the above reasons, hyperthermia therapy is usually carried out at a temperature in the range of 42–47 °C. Cancer cells will be killed in a time- and temperature-dependent manner.[29] Although the exact mechanism of cell killing by hyperthermia is still unclear, many reports indicate that protein denaturation is the key event in the disruption of cellular homeostasis.[30] For different types of cells, the onset temperatures for protein denaturation vary. When the temperature rises beyond 41 °C, protein denaturation will occur in a variety of organelles, including microsomal membranes, mitochondria, cytosol, nucleus, and nuclear matrix.[30–32] The protein denaturation will directly cause the inactivation of enzymes and reducing the binding capability of membrane receptors.[33] It was shown that denaturation of 10% of the cellular proteins would cause over 95% of V79 cells to die, whereas nearly no killing effect was observed when the level of denaturation was below 5%.[32] In addition to the direct cytotoxic effect, hyperthermia will impair the supply of oxygen and nutrients and thereby alter the tumor microenvironment due to the collapse of tumor vasculature and the decrease of blood flow when the temperature is raised above the critical point of vascular stasis. Taken together, hyperthermia in the temperature range of 42–47 °C offers an effective means for cancer treatment.[34]

When the temperature is beyond 48 °C, thermal ablation typically occurs at local sites. Irreversible damages to critical cellular proteins, vasculature, and tissue structural components will appear within a few minutes at such high temperatures. The mechanism of thermal ablation differs from what is involved in hyperthermia therapy. The high temperature will induce drastic activation of cell death and coagulative necrosis. Denaturation of proteins, inactivation of enzymes, collapse of cell membrane, and dysfunction of mitochondria can all be observed.[35] At temperatures above 60 °C, immediate cellular destruction occurs irrespective of the tissue histology. Meanwhile, the time needed to achieve irreversible damage decreases exponentially.[36] Thermal ablation offers a number of advantages for cancer treatment, but its capability is often limited by factors such as temperature heterogeneity inside the tumor and potential overheating of the surrounding healthy tissues.

3. The Irradiation Source for PTT

The ability of electromagnetic waves to penetrate through tissues is crucial to their use in both diagnostics and therapy. The propagation of an electromagnetic wave in a biological tissue is determined by the fundamental optical properties of the tissue, including absorption coefficient (μ_a), scattering coefficient (μ_s), anisotropy coefficient (g), and index of refraction (n).[37] These properties depend on the wavelength of the electromagnetic wave and vary between tissues owing to their different compositions (Figure 2A). For γ- and X-rays, both of them have extremely short wavelengths with high energies and can ionize the outer electrons, leading to high transparency *in vivo*. Light with wavelengths longer than X-ray is nonionizing and can be divided into two types according to their scattering and absorption by the tissues. Radiations from 1 MHz to 300 GHz (microwave and radio waves) with wavelengths comparable to the size of cells exhibit little scattering by tissues.[38] However, significant scattering and molecular absorption will be observed in tissues for light with wavelengths in the range of 0.2–100 μm (ultraviolet, visible, NIR, and infrared).[37,38] The strong absorption is mainly caused by the interaction between light and tissue when the photon energy matches the energy gaps involved in electronic, vibrational, and translational transitions of the molecular species in tissue.

The penetration depth of ultraviolet (UV) light in skin is typically no more than 200 μm due to the high absorption and scattering coefficients (Figure 2B).[39,40] Therefore, UV is usually used for superficial diseases such as skin infections and wound healing. For the visible light, the absorption coefficients of tissues vary greatly, while the scattering coefficients decrease monotonically as the wavelength increases (Figure 2C).[39,40] The absorption coefficient of tissue is mainly determined by a variety of components with distinct absorption spectra, including blood, water, melanin, lipid, bilirubin, and beta-carotene (Figure 2D).[37] Among these, blood and water are responsible for the light absorption of tissue. The light absorption by blood in the region of 400–650 nm mainly originates from hemoglobins.[37,42] Water is nearly transparent in the region of visible light and becomes absorbing over the NIR region.[37] Due to the significantly-increased absorption of blood at shorter wavelengths and that of water at longer wavelengths, two transparent windows in the NIR region (650–950 nm and 1000–1350 nm) are typically used for PTT, as well as for *in vivo* optical imaging (Figure 2D).[14,15,43] Second NIR light (NIR-II) is reported to possess better biological transparency, deeper penetration, less energy dissipation and minimal normal-tissue toxicity.[44–46]

Infrared light can only penetrate several millimeters into soft tissues because of the strong absorption of water in the infrared region (Figure 2E). As the wavelength increases, the absorption of water decreases in the microwave region (Table 1),[38] so the penetration depth increases significantly. Microwave is largely transparent to soft tissues and can penetrate several centimeters into those with low water contents. Far-infrared and microwave radiations will excite the vibrational and rotational modes of water molecules and thus generate heat (Figure 2A). Due to a good combination of penetration depth and heat generation, microwave has also been used for hyperthermia therapy. When the wavelength is increased to one meter (<300 MHz in frequency, radio region), the radiation becomes transparent to water again (Figure 2E).[37,47]

4. Photothermal Transducers

4.1. Photothermal Conversion Efficiency

Upon the irradiation of a photothermal transducer with NIR light, some of the incident photons will be scatted while some of them will be absorbed. The extinction of light is determined by both scattering and absorption. The absorption efficiency (Φ_{abs}) is defined as the ratio of absorption coefficient (α_{abs}) to extinction coefficient ($\alpha_{ext}=\alpha_{abs}+\alpha_{sct}$), that is, $\Phi_{abs} = \alpha_{abs}/\alpha_{ext}$..[48] The extinction coefficient is related to the concentration (N) of illuminated NPs and the extinction cross section (σ_{ext}) by: $\sigma_{ext}= \alpha_{ext}/N$.

To measure the absorption efficiency of the photothermal transducers, theoretical and experimental methods have been developed. As a conventional method, UV-vis-NIR spectrometer has been widely used to determine the extinction spectra of photothermal transducers. In general, one has to rely on theoretical calculations to separate the extinction coefficient into scattering and absorption components. In this respect, the Mie theory can be applied to spherical particles, while the discrete-dipole approximation (DDA) method is typically used for nanostructures with other geometric shapes. Using DDA method, the scattering and absorption spectra of gold nanocages and nanoboxes with four different sets of geometric parameters have been investigated (Figure 3). The results indicate that gold nanoboxes with a smaller size exhibit a higher absorption coefficient than larger ones owing to the decrease in scattering component.[49,50] This phenomenon has also been observed in both gold nanospheres and nanorods.[51,52]

To experimentally measure the photothermal conversion efficiency, several techniques have been developed. Our group demonstrated the use of photoacoustic imaging to experimentally measure the absorption coefficients of gold nanostructures. The almost linear correlation between photoacoustic signal and absorption coefficient makes this mothed ideal for the determination of photothermal conversion efficiency.[53] To derive the photothermal conversion efficiency more conveniently, we also developed a simple device based on plasmon-assisted optofluidic technology. The efficiency can be calculated by measuring the volumetric expansion of a suspension containing the transducers in a glass capillary.[54] With this homemade system, the absorption coefficients and photothermal conversion efficiencies of gold nanocages, nanorods, and hexapods were measured and compared. Double beam fluorescence thermometry has also been reported as an adequate and reliable technique for determining the absorption coefficients of photothermal transducers. Using thermosensitive fluorescent quantum dots as a sensor, the absorption and photothermal heating efficiency of gold nanoparticles with different morphologies (nanorods, nanocages, nanoshells, and nanostars) were obtained.[55]

4.2. Diversity of Nanomaterials

An ideal photothermal transducer should have both a large absorption coefficient and a high absorption efficiency in the NIR region, together with a low quantum yield for luminescence to ensure efficient light-to-heat conversion. In addition, the photothermal transducer should be biocompatible, nontoxic, and capable of accumulating inside the solid tumor. A wide variety of photothermal transducers have been developed and successfully applied to PTT. Table 2 shows a partial list of the reported transducers, which can be divided into subgroups in different ways: for example, inorganic *vs.* organic, metallic *vs.* semiconducting, and nanoscale *vs.* molecular. Depending on the composition and structure, the molar extinction coefficients and absorption efficiencies of the photothermal transducers can differ significantly.

Inorganic photothermal transducers include nanostructures made of Au, transition metal dichalcogenides, and many other types of materials. Owing to their tunable localized surface plasmon resonance (LSPR) in the NIR region, gold nanostructures such as nanorods, nanostars, nanoshells, nanoboxes, and nanocages have all been extensively explored for PTT. The LSPR properties of Au nanostructures are strongly affected by their size, shape, and structure (solid *vs.* hollow). Hence, the absorption peaks can be tuned into the NIR region by varying the aspect ratio (length/width) for nanorods and nanostars or shell thickness/composition for nanoshells, nanoboxes, and nanocages.[11,48,49,68–71] As shown in Figure 4, the increase of aspect ratio or reduction in shell thickness will cause a red-shift to the LSPR peak. On the other hand, the physical dimensions of the nanostructures can affect the absorption efficiency.

Carbon nanomaterials, including single-walled carbon nanotubes (SWCNTs), multi-walled carbon nanotubes (MWCNTs), and graphene and its derivatives, have also been actively explored for PTT. The absorption of SWCNTs in the NIR region (650–1600 nm) is due to the "Van Hove transitions", while the absorption in the UV-vis region (450–650 nm) originates from the π plasmon resonance.[71,73] The photothermal conversion occurs during the de-excitation processes between Van Hove states.[48] Luminescence is also observed at the same time, albeit the quantum yield is very low (usually, below 1%).[74] Carbon-based nanomaterials with various morphologies display strong, continuous absorption over a broad region of 700–1200 nm. This is quite different from Au nanostructures, which are typically limited to the relatively narrow LSPR peaks.[48,75]

Although both Au- and carbon-based nanostructures are promising for clinic application owing to their bio-inertness, their long-term metabolism has raised concerns because of their non-biodegradable nature. To address this issue, transition metal sulfides and oxides, such as CuS,[76] MoS_2,[77] and WS_2[78] have emerged as a new class of inorganic photothermal transducers. When prepared as nanostructures, the NIR absorption of these materials can be mainly attributed to LSPR. According to an *in vivo* study, about 90% of the CuS hollow nanoparticles could be eliminated through hepatobiliary and renal excretion within one month post intravenous injection, while only 2.3% of Au hollow nanospheres with a similar size and morphology was eliminated.[79] Besides, changes to the liver tissue caused by the CuS hollow nanoparticles were reversible, while the Au hollow nanospheres led to irreversible changes in terms of proteomic profile because of the non-metabolizability of Au.

Many organic photothermal transducers with good biocompatibility have also been developed and explored for PTT. Porphysomes—nanoparticles self-assembled from phospholipid-porphyrin conjugates—possess a liposome-like structure and exhibit strong absorption of NIR light due to the inclusion of porphyrin unit. The porphysomes can overcome the drawback of small extinction coefficients associated with the traditional organic dyes, exhibited an extremely large coefficient of 2.9×10^9 M^{-1} cm^{-1} (ε_{680}) due to the high porphyrin packing density. Besides, the absorption peak and extinction coefficient can be tuned by employing different types of porphyrins.[64] Other organic materials such as polyaniline (PANi),[61,80] polypyrrole (PPy),[60,81] naphthalenediimide-based metal-organic,[82] quaterrylenediimide,[83] and phenothiazinium[84] have also been explored. During the synthesis, doping with suitable materials (usually, transition metals, acids, and alkali ions) is important for achieving absorption in the NIR. After doping, inter-band states between the valence and conduction bands will be generated to increase the mobility of electrons and reduce the energy gap, resulting in a red-shift for the absorption peak to the NIR.[85] Nanoparticles made of conjugated polymers exhibit large extinction coefficients, which are significantly greater than the conventional organic dyes, and can even become comparable to inorganic materials. The last but not least, small NIR dye molecules such as indocyanine green (ICG),[86] IR 780,[87] IR 808,[88] have all been explored as efficient photothermal transducers for PTT. They are typically loaded in organic carriers such as liposomes, polymer nanoparticles, micelles, and protein nanoparticles. Their encapsulation in nanoparticles can reduce the elimination rate, improve the photostability relative to free dyes, decrease the side effects, and increase tumor accumulation.

4.3. Photostability during PTT

During PTT, the tumor usually needs to be irradiated with the NIR light several times. An ideal photothermal transducer should not only have a high absorption efficiency and low toxicity but also great stability during the irradiation for continuously generating therapeutic effect. As widely used photothermal transducers, the photostability of Au nanostructures is quite different under continuous-wave (CW) and pulsed laser. Under the irradiation of CW laser, Au nanocages and nanostars were very stable,[89,90] while Au nanorods tend to be photobleached after long time irradiation.[91] Due to the extremely high energy of a pulsed laser, various kinds of Au nanostructures will be destroyed. For example, Au nanocages,[92] nanorods,[93] and nanoshells,[94] all melted and evolved into spherical particles upon the irradiation with a nanosecond or femtosecond pulse laser, accompanied by the disappearance of absorption in the NIR region and appearance of absorption in the visible region. The laser-induced melting of Au nanorods is dependent on both the laser energy and pulse width. At moderate energies, the femtosecond laser melted the nanorods to nearly spherical particles of comparable volumes while the nanosecond laser fragmented the nanorods into smaller, near-spherical particles. At high energies, fragmentation was also observed for the case of femtosecond laser.[93] The photothermal instability of Au nanostructures is owing to the physical deformations caused by extremely high temperatures within a short period of time.[93] By coating or grafting with other materials, the photostability of Au nanostructures can be improved significantly. For example, the photostability of Au nanorods was substantially improved after coating with silica. Besides, increase the thickness of the silica shell could further improve the stability of Au nanorods.[95] Reduced graphene oxide has also been used to enhance the photostability of Au nanorods when applied as a shell.[96]

For nanoparticles made of conjugated polymers such as PANi[61] and PPy,[97] they are able to survive a long period of irradiation with continuous-wave laser. Being comprised of organic dyes, porphysomes are potentially photobleached under irradiation. However, when Mn^{2+} was incorporated to generate Mn-porphysomes, the photostability was improved significantly when compared to the original system.[98] Free NIR dyes such as ICG and IR 780 tend to be photobleached after irradiation with continuous-wave laser for several minutes. As such, they are rarely used for PTT in the form of free molecules. By loading them into nanoparticles, the photostability can be greatly improved.[99,100] In general, packaging or coating with other materials to form hybrid structures is a feasible approach to improving the photostability of most photothermal transducers.

5. Optimize the Distribution of Photothermal Transducers in the Tumor

5.1. Extravasation and Accumulation of Nanoparticles in the Tumor

Though successful to a certain extent, cancer recurrence can still occur post PTT. This can be partially attributed to the limited intra-tumoral accumulation of photothermal transducers, as well as their inhomogeneous distributions due to the disorganized vascularity in a solid tumor and their inefficient uptake by cancer cells (Figure 1).

Upon intravenous injection, only a small fraction of the transducers will be accumulated inside the tumor; the majority is likely subjected to the mononuclear phagocyte system (MPS)-mediated elimination or excretion through kidney when featuring a size smaller than 5.5 nm.[101] To mitigate MPS clearance, PEGylation—surface modification with poly(ethylene glycol) (PEG) chains in either covalent or non-covalent manner—has been broadly applied to render the nanoparticles with a stealth property by reducing the formation of protein corona.[102] The efficiency of delivery is also dependent on the particle size. The rapid growth of tumor tissue leads to the formation of pores in the immature tumor blood vessels, which are permeable to nanoparticles. The cutoff size of the pores varies from 400–600 nm to several micrometers depending on the tumor type, indicating that nanoparticles smaller than 400–600 nm should have no problem to extravasate into the tumor matrix.[103–105] Meanwhile, the uptake by liver and spleen, two major MPS organs, and the resultant clearance are also size-dependent. Specifically, particles smaller than 50 nm can pass through the liver vessels and interact with hepatocytes, whereas particles greater than 400 nm in size will be likely eliminated by the spleen.[103] As such, nanoparticles with sizes in the range of 100–200 nm are generally believed to be optimal for increasing tumor accumulation and reducing MPS clearance.[106] Of course, there are always exceptions. For example, the amount of Fe_3O_4 nanoparticles with a diameter of 310 nm accumulated in a solid tumor was much greater than its smaller counterparts (*e.g.*, 60, 120, or 200 nm), suggesting that the intra-tumoral accumulation of particles was not solely determined by the particle size.[107]

It was reported that the surface charge on nanoparticles also played an important role in regulating their pharmacokinetics and biodistribution. In particular, nanoparticles with a more positive zeta-potential (ξ >10 mV) tend to suffer from a remarkable reduction in blood availability due to the serious aggregation effect between the positively charged particles and the negatively charged proteins, leading to non-tolerable side effect. For negatively-charged particles (ξ <−10 mV). they tend to be recognized and cleared by MPS. For nearly neutral particles (−10 mV to +10 mV), they have been proven to feature a longer blood half-life, and thus a greater level of accumulation in tumors.[106,108] Furthermore, growing evidences suggest that the shape or morphology of nanoparticles can also affect their fate *in vivo*. As an example, our group investigated the shape-dependence of biodistribution and pharmacokinetics by focusing on a set of Au nanostructures including nanohexapods (50 nm), nanorods (9×36 nm), and nanocages (47 nm). It was shown that anisotropic nanostructures such as nanorods and nanohexapods were accumulated more efficiently with respect to isotropic nanostructure like nanocages at 24 h post administration (8.4, 7.2, and 2.6% injected dose/g tumor tissue for nanorods, nanohexapods, and nanocages, respectively).[57]

5.2. Penetration and Diffusion of Nanoparticles in the Tumor

Although nanoparticles with appropriate sizes can accumulate in the tumor efficiently, it is still hard to realize a homogenous distribution throughout the tumor. A large portion of the particles only accumulate at the periphery of a tumor where abundant vessels in high perfusion speed exist, leaving the poorly vascularized, hypoxic inner tumor tissue less populated by the particles. This would greatly reduce the treatment efficacy and provide a strong driving force for recurrence. Investigations suggest that the limited penetration of nanoparticles can be partially attributed to the increased interstitial fluid pressure caused by the dysfunctional lymphatics system in the tumor, as well as the stiff extracellular matrix.[109] Particularly, a high interstitial fluid pressure will likely increase the outflow of proteins together with other molecules from the tumor interstitial vessels to the blood stream, disrupting the distribution of particles that rely largely on the convective flow.[110] The tumor extracellular matrix, which is composed of elastic collagen fibers and a network of proteins and glycosaminoglycans, plays a crucial role in determining the penetration of nanoparticles. The content of collagen in tumors is higher than that in normal tissues, and is cross-linked by the increased level of lysyl oxidase, contributing collectively to a denser and stiffer tumor extracellular matrix.[109] Besides, it is worth noting that mean tumor inter-capillary distances generally range from approximately 80 to hundreds of micrometers, presenting another obstacle to prevent nanoparticles from reaching tumor cells that are away from vessels.[111,112] As such, nanoparticles smaller in size hold greater promise relative to their large counterparts in terms of penetration ability except for the ultrafine particles (<5.5 nm), which will be subjected to renal clearance as mentioned above.[113,114]

Based on our evaluation, Au nanocages with a size of approximately 48 nm could penetrate deeply into the inner portion of the solid tumor post intravenous injection. The amount of accumulation at the tumor boundary and in the center differ by more than two folds, indicating a heterogeneous distribution as expected.[114] In a different study, the distributions of various Au nanoparticles differ in size were also visualized under a microscope through silver enhancement.[115] At 8 h post injection, a size-dependent accumulation was observed, in which the migration of 20-nm particles toward the interstitial space was the longest in all the groups tested, whereas the 60- and 100-nm particles tended to be entrapped perivascularly.[115]

Considering that nanoparticles with larger sizes are better for tumor accumulation and retention, while nanoparticles with smaller sizes are more suitable for tumor penetration, size-switchable nanoparticles were developed to simultaneously realize both high accumulation and homogeneous distribution inside a tumor.[116–118] To this end, nanoclusters based on tetrachloroperylene monoamide were developed for deep penetration, which could disassemble into smaller particles when triggered by carboxylesterase (Figure 5A).[118] The size of the nanoclusters was switched from ~100 nm to ~10 nm (Figure 5B) after dispersion in carboxylesterase solution for 12 h, making them distributed more uniformly inside a tumor (Figure 5C). In another study, size-switchable micelles were developed from pH-sensitive poly(4-formylphenyl methacrylate-co-2-(diethylamino) ethyl methacrylate)-b-polyoligoethyleneglycol methacrylate (P(FPMA-co-DEA)-b-POEGMA).[119] The polymer was amphiphilic at pH=7.4 and became hydrophilic at pH=6.6 (Figure 5D). The micelles showed a significant change in size from 126.3 ± 5.6 nm at pH=7.4 to 12.1 ± 0.9 nm at pH=6.6 (Figure 5E). The penetration capability could be greatly enhanced at pH=6.6 due to the major reduction in size (Figure 5F).

In addition to particle size, the surface charge also plays a pivotal role in affecting the penetration of nanoparticles. Specifically, neutral nanoparticles (ξ potential: ± 10 mV) are much less vulnerable to the extracellular matrix-mediated entrapment caused by the protein-particle interaction than their highly-charged counterparts,[120] leading to deeper penetration and more homogeneous distribution. Furthermore, surface functionalization with targeting moieties will provide the nanoparticles with additional affinity toward specific cells expressing certain receptors, and thus allow for deeper penetration than passive accumulation.[121]

5.3. Cellular Internalization of the Nanoparticles

Although the effect of PTT is independent of nanoparticle internalization, efficient cellular uptake will make cancer cells more sensitive to heat, increasing the therapeutic efficiency. It was reported that the internalized Au nanorods could induce necrotic cell death at a rate much faster than it was achieved using nanoparticles bound to plasma membrane only.[122,123] A similar effect was also observed when using carbon nanotubes as the photothermal transducer.[124] Collectively, these results support the notion that internalization of photothermal transducers plays a crucial role in PTT. Given that nearly all organelles and cellular components (*e.g.*, DNA and protein) are susceptible to heat stress and they are located inside cells, it is reasonable to understand why the internalized nanoparticles tend to outperform those bound to plasma membrane only during PTT.

The size of nanoparticles also plays a dominant role in affecting the cellular internalization in terms of speed and efficacy. Particles ranging from a few nanometers to a few micrometers (up to 5 μm) can be internalized by cells through distinct energy-consuming mechanisms. Particularly, large particles (especially, those with sizes over 1 μm) can be readily internalized by phagocytic cells through a process known as micropinocytosis, whereas small particles are favored by non-phagocytic cells.[125,126] The size-dependence of nanoparticle uptake has been extensively studied. As an example, the internalization of Au nanoparticles with a diameter of ~50 nm by cells is more efficient than smaller (14 or 30 nm) or larger (74 nm or100 nm) counterparts *via* receptor-mediated endocytosis (Figure 6A).[115] Iron oxide nanoparticles also exhibit size-dependent cellular uptake as particles of 37 and 65 nm in diameter were internalized faster than the 8- and 23-nm counterparts.[127] When the particle size was increased from 60 to 300 nm, the internalization efficacy dropped drastically, implying the presence of complicated interplay between the particle size and the endocytic behavior.[107] The limited uptake of very small or large nanoparticles may be caused by the down-regulation of a specific receptor so that nanoparticles of certain sizes can efficiently activate endocytic cascade through their ability to adjust the distribution of potential receptors (Figure 6B–C).[128] Although small particles showed a lower internalization efficacy than that of 40–60 nm, ultrasmall (<6 nm) particles tend to accumulate in the nucleus and are useful for nucleus gene and drug delivery.[129–131]

The shape of nanoparticles also affects their manner of cellular internalization. For example, the uptake of rod-shaped Au nanostructures by cells is lower than the spherical counterparts, and the internalization efficacy has a negative correlation with their aspect ratio.[115] As shown by computational analysis, the cellular uptake of anisotropic nanostructures such as nanorods is not energy favorable due to the formation of endocytic vesicles bearing large curvature. This trend is consistent with the observation that even Au nanohexapods and nanocages could be internalized more efficiently than nanorods under identical conditions (Figure 6D).[57]

For both phagocytic and non-phagocytic cells, positively-charged nanoparticles are generally more efficient for internalization through the electrostatic interaction relative to neutral and negatively-charged particles. Surface modification such as PEGylation is usually used to avoid the recognition and clearance by macrophages for generating a strongly-hydrophilic coating, but it will also sterically prevent nanoparticles from accessing the cancer cell. In an aim to address this issue, several strategies, including the introduction of pH-sensitive bonds,[132] and matrix metalloproteinase cleavable peptides,[133] have been proposed to intelligently remove the PEG coating once they have entered into the tumor microenvironment.

6. Challenges in PTT

For the application of PTT in clinic, it should be noted that although exciting outcomes have been achieved, PTT is presently in the proof-of-concept stage. Nanomaterials with good biocompatibility and high targeting ability for malignant tumors is in urgent need for clinical applications. Since, most of the nanomaterials are located in reticuloendothelial system, while only a small fraction could be accumulated in the tumor regions.[134] What’s more, a uniform distribution of the photothermal transducers is a prerequisite for the homogeneous generation of heat during the PTT, but it has been difficult to accomplish in many cases. In addition, several other challenges may also arise when regulating the intra-tumoral heat distribution and improving the therapeutic effect, including blood vessel perfusion, tumor size, the location of photothermal agents, the thermal conductivity of tumor microenvironment, as well as the real-time temperature monitoring.

6.1. Heat-Sink Effect

The highly-vascularized peripheral tumor section has been shown to reduce the potency of the thermal effect because of the heat-sink effect, with respect to the inner tissue of a solid tumor.[135,136] Specifically, the high blood perfusion rate of the vessels can lead to rapid dissipation of heat, making it hard to realize the eradication of tumor lesions near a large vascular structure, and this is known as the heat-sink phenomenon.[137] During PTT, the abundant vasculature will result in more accumulation of the photothermal transducers and thus high temperature upon NIR irradiation.[138] On this basis, more efforts should be paid to the inner part of the solid tumor instead of the peripheral region. In contrast, traditional hyperthermia approaches such as radiofrequency ablation (RFA) and high intensity focused ultrasound (HIFU) usually elevate the temperature in the focused center rather than in the peripheral region. The complementary heating effect of RFA or HIFU and PTT indicates the potential of combined hyperthermia therapy.

6.2. Tissue Heat Conductivity

Considering the difficulty of photothermal agents in realizing a homogeneous intra-tumoral distribution, the elevation of local temperature in areas containing less accumulation is thus governed primarily by the conductivity of the generated heat. In particular, poor heat dissipation limits the heating of tissues surrounding irradiated lesions and lead to sections differing in temperature. The content of water has been proven to be correlated tightly with the heating profiles in tumor tissues due to the fact that water molecules are a superior conductor for heat. Specifically, a water content over 50% has been proven to be capable of remarkably mitigating the heterogeneity of heat distribution.[43] Given the distinct profiles of water content and resultant thermal conductivity of malignant and normal cells (*e.g.*, the thermal conductivity of neuroblastoma and fat account for 89% and 39% of that of water),[139–141] it is possible to achieve specifical tumor destruction. Notably, though the thermal conductivity of the medium shows a positive correlation with the temperature, tumors experiencing PTT operated at extremely high temperatures will suffer from rapid protein denaturation as well as water vaporization, and in turn decrease the thermal conductivity,[142] which should be avoided in practical applications.

6.3. Thermotolerance

When cells are exposed to hyperthermia temperature for a short period of time (ranging from 10 to 30 min), followed by cooling down to 37 °C or exposure to mild hyperthermia temperatures for a long duration of time, thermal resistance (known as thermotolerance) will occur. Once the stress stimulus is removed, cells can recover their normal cellular function. Thermotolerance is generally associated with the generation of heat shock proteins, which play a key role in protecting the cells from the elevated temperatures by binding to newly denatured proteins to block aggregation and allowing the proteins to refold.[143] Heat shock proteins not only protect the tumor cells from the elevated temperatures but also other stresses such as ischemia, drug, and reactive oxygen species (ROS).[144,145] They exhibit diverse functions and are expressed at high levels in tumors. When they are generated inside the cells, they can keep the cells survive by inhibiting apoptosis.[146] When they are released into the extracellular matrix by necrotic cells, they will engage in various immunological processes, as tumor antigens chaperones to stimulate specific tumor immunity and lead to tumor regression.[147] However, it was reported that only the heat shock proteins isolated from cancer cells, not those from normal tissues, were able to induce the tumor immunity.

To overcome the thermotolerance caused by heat shock proteins, inhibitors can be co-delivered into the tumor together with photothermal agents to greatly enhance the therapeutic efficacy. To this end, it was shown that copper sulfide could reduce the overexpression of heat shock protein 90 (HSP90) and were used with PTT to generate a synergistic effect.[148] Besides, the heat shock proteins generated during PTT can also be used as a target for efficient delivery of chemotherapeutics into the tumor.[149] After moderate hyperthermia (*e.g.*, 43 °C for 30 min), heat shock proteins-targeted conjugates exhibited a significantly greater inhibition effect against cancer cells.

6.4. Attenuation of Light in the Tumor

Although homogenous dispersion of the nanoscale transducers in tumor tissue will improve the photothermal effect, the attenuation of light caused by the absorption and scattering of the transducers themselves will inevitably reduce the light intensity at positions deep inside the tumor, leading to insufficient heat generation. This effect will limit the therapeutic efficacy and cause the recurrence of the tumor. Taken together, both homogenous dispersion of the transducers and adequate light irradiance are necessary for an effective treatment. Simply increasing the power will cause overheating to the surface of a tumor and damage the adjacent tissues. To address this challenge, reversible thermochromic nanoparticles have been fabricated to regulate light transmission and photothermal heating with a pre-defined set-point for temperature.[150,151] The nanoparticles were colored at low temperature and conversed to a colorless state at 45 °C, the transition temperature (Figure 7A). The colored nanoparticles could transfer the NIR light to heat and maintain the temperature at 45 °C (Figure 7B). When reaching the transition temperature, the colorless nanoparticles allowed deeper penetration of the light, preventing overheating during the PTT (Figure 7C–E). To this end, auto-regulated liposomes containing J-aggregates (JAG) were developed to regulate light transmission during the PTT.[152] With the use of a temperature-responsive host lipid, the absorption of the photothermal transducer can be adjusted. Under the irradiation by NIR light, deeper layers of the target tissue revert to the intrinsic optical absorption, halting the temperature rise and enabling greater light penetration and heat generation at a great depth.[152]

6.5. Monitoring of Temperature

The efficacy of PTT may differ between individuals and tumor entities.[153] Some tumors are “easy-to-heat”, while others are “difficult-to-heat”. Consequently, the temperature, which is critical to hyperthermia therapy, will differ significantly in different tumors even under the same thermal dose. Therefore, a non-invasive method for real-time monitoring of 3D temperature distributions during the treatment will greatly enhance the ability to uniformly heat the tumors at therapeutic levels. Novel techniques for non-invasive measurement of temperature have appeared in recent years, including electrical impedance tomography (EIT),[154] microwave radiometry,[155] computer tomography (CT),[153] magnetic resonance imaging (MRI),[156] afterglow,[157] and ultrasound.[158]

Magnetic resonance imaging (MRI) has been used to monitor temperatures for more than one decade due to the high contrast and spatial resolution. MR thermometry can be carried out based on three temperature-sensitive parameters: the relaxation time T_1, the diffusion coefficient (apparent diffusion coefficient value, D), or the proton resonance frequency shift.[159] The method based on relaxation time T_1 is strongly dependent on the type of tissue and is mainly recommended in low-field systems.[160] On the contrary, the method based on diffusion coefficient is highly sensitive to temperature. However, it needs a long time to acquire data due to the high sensitivity to motion.[161] Proton resonance frequency-based temperature monitoring, which relies on the resonant frequency shift of water proton, is preferred by most investigators. It exhibits good linearity and temperature sensitivity at mid to high field strengths (≥1 T).[162] Besides, this method shows a satisfactory standard deviation of less than 1 °C with temporal resolution below 1 sec and a spatial resolution of about 2 mm, for a single slice of immobile tissue. However, this method is inappropriate for lipid tissues, since there is no hydrogen bonding among the methylene protons that supply the bulk of fat signal.[163]

Compared with MRI, ultrasound thermometry is a portable, inexpensive, and convenient technique for guiding hyperthermia therapy, especially for intracavitary and endoluminal applications.[164] Several ultrasonic parameters sensitive to temperature have been used for estimating the temperature of tissue, including the echo-shifts caused by thermal expansion and speed of sound, the frequency-dependent acoustic attenuation coefficient, and the backscattered energy from tissue inhomogeneities.[165,166] Although ultrasonic thermometry has not been used for measuring large temperature variation, it is sensitive to small (<1 °C) temperature change, together with high spatial sampling and high temporal resolution, suggesting the greatest potential for monitoring temperatures in the hyperthermia range.[164,167]

Recently, fluorescence has also been applied for *in vivo* temperature determination. To this end, a nanodiamond quantum thermometry system was reported for *in vivo* temperature monitoring (Figure 8A).[168] The frequency shift of the optically-detected magnetic resonance (ODMR) of nitrogen-vacancy (NV) defect centers in the nanodiamond was sensitive to temperature and could be measured as a decrease in the laser-induced fluorescence intensity when spin-resonant microwave excitation was applied (Figure 8B). After injection of the nanodiamonds, the fluorescence could be observed in the worm (Figure 8C). By determining the temperature-dependent continuous-wave (CW)–ODMR spectrum, the real-time temperature was measured (Figure 8D and E). This method showed good *in vivo* precision and accuracy of ± 0.22 °C and <0.6 °C, respectively. In another study, a temperature-feedback probe based on carbon-coated core-shell upconversion nanocomposite $NaLuF_4$: Yb, Er@$NaLuF_4$@carbon (csUCNP@C) was developed for PTT.[169] The upconversion nanocomposite could convert the lower-energy light at 980 nm into higher energy emissions in a temperature-dependent manner (Figure 8F). The higher temperature resulted in a higher upconversion luminescence ratio between 525 nm and 545 nm. During PTT, cells with upconversion luminescence were killed, whereas the others without upconversion signals were still alive, suggesting that the luminescence could be used as an indicator of temperature elevation. (Figure 8G).

7. Conclusions

In summary, to realize effective PTT, various factors such as the light source, properties of the photothermal transducers, as well as tissue characteristics all need to be taken into consideration. For the photothermal transducers, we shall not only pay attention to their absorption coefficient, photothermal conversion efficiency, and photostability, but also the size, shape/morphology, and surface charge. For tissue characteristics, the heat-sink effect, thermal conductivity, and thermotolerance should be taken into account. With the continuous development of novel photothermal transducers and temperature monitoring techniques, PTT will become more efficient and precise in cancer-specific therapy. Besides, the distinct features of PTT also provide opportunities for combination therapy by integrating with other types of treatment. For example, the increased temperature and blood flow in tumors during PTT will accelerate drug release and promote the diffusion of the drug, offering a platform to integrate with chemotherapy. At the same time, the homogeneous distribution of heat in PTT holds promise for the synergistic effect with RFA or HIFU in tumor therapy.

Acknowledgements

This work was supported in part by the NIH Director's Pioneer Award (DP1 OD000798), a research grant from the NIH (1R01 CA138527), start-up funds from the Georgia Institute of Technology, and National Natural Science Foundation of China (82272662).

Biographies

Song Shen received his Ph.D. in pharmaceutics from Zhejiang University in 2014. He joined the Xia group at the Georgia Institute of Technology as a visiting scholar in 2016. He is currently a professor at the College of Pharmaceutical science at Jiangsu University. His research interest includes the nanomaterials for bio-application and smart drug delivery systems.

Jichuan Qiu received his Ph.D. in materials chemistry and physics from Shandong University in 2018 with Prof. Hong Liu. He joined the Xia group at the Georgia Institute of Technology as a visiting graduate student in 2016 and then continued as a postdoctoral fellow since 2018. He is currently a professor in the State Key Laboratory of Crystal Materials at Shandong University. His research interest includes the design and rational synthesis of nanostructured materials for biomedical applications.

Younan Xia studied at the University of Science and Technology of China (B.S., 1987) and University of Pennsylvania (M.S., 1993) before receiving his Ph.D. from Harvard University in 1996 (with George M. Whitesides). He started as an assistant professor of chemistry at the University of Washington (Seattle) in 1997 and was promoted to associate professor and professor in 2002 and 2004, respectively. He joined the Department of Biomedical Engineering at Washington University in St. Louis in 2007 as the James M. McKelvey Professor. Since 2012, he holds the position of Brock Family Chair and GRA Eminent Scholar in Nanomedicine at the Georgia Institute of Technology.

References

[1]. Ijff M, Crezee J, Oei AL, Stalpers LJA, Westerveld H, Int. J. Gynecol. Cancer 2022, 32, 288–296. [PubMed: 35046082]

[2]. Liebl CM, Kutschan S, Doerfler J, Kaesmann L, Hubner J, Clin. Exp. Med. 2022, 22, 519–565. [PubMed: 35767077]

[3]. Deng Z, Jiang C, Younis MR, Lei S, He Y, Zheng H, Huang P, Lin J, Chin. Chem. Lett. 2021, 32, 2411–2414.

[4]. Sun Y.-d., Zhang H, Liu J.-z., Xu H.-r., Wu H.-y., Zhai H.-z., Lu C.-y., Zhao X, Chen Y.-q., Zhou L.-l., Han J-J, Thoracic Cancer 2019, 10, 543–550. [PubMed: 30677240]

[5]. Jeanjean P, El Hamrani D, Genevois C, Quesson B, Couillaud F, Adv. Mater. Technol. 2022, 7, 2101258.

[6]. Mai X, Chang Y, You Y, He L, Chen T, J. Controlled Release 2021, 331, 270–281.

[7]. Ximendes E, Marin R, Shen Y, Ruiz D, Gomez-Cerezo D, Rodriguez-Sevilla P, Lifante J, Viveros-Mendez PX, Gamez F, Garcia-Soriano D, Salas G, Zalbidea C, Espinosa A, Benayas A, Garcia-Carrillo N, Cusso L, Desco M, Teran FJ, Juarez BH, Jaque D, Adv. Mater. 2021, 33, 2100077.

[8]. Yu Y, Tang D, Liu C, Zhang Q, Tang L, Lu Y, Xiao H, Adv. Mater. 2022, 34, 202105976.

[9]. Li S, Deng Q, Zhang Y, Li X, Wen G, Cui X, Wan Y, Huang Y, Chen J, Liu Z, Wang L, Lee C-S, Adv. Mater. 2020, 32, 2001146.

[10]. Qiu J, Liu Y, Xia Y, Adv. Healthc. Mater. 2021, 10, 2002031.

[11]. Qiu J, Xie M, Wu T, Qin D, Xia Y, Chem. Sci. 2020, 11, 12955–12973.

[12]. Yu S, Zhou Y, Sun Y, Wu S, Xu T, Chang Y-C, Bi S, Jiang L-P, Zhu J-J, Angew. Chem. Int. Ed. 2021, 60, 5948–5958.

[13]. Yi W, Xiao P, Liu X, Zhao Z, Sun X, Wang J, Zhou L, Wang G, Cao H, Wang D, Li Y, Signal Transduct. Target. Ther. 2022, 7, 386. [PubMed: 36460660]

[14]. Chang B, Li D, Ren Y, Qu C, Shi X, Liu R, Liu H, Tian J, Hu Z, Sun T, Cheng Z, Nat. Biomed. Eng 2022, 6, 629–639. [PubMed: 34385694]

[15]. Smith AM, Mancini MC, Nie SM, Nat. Nanotechnol. 2009, 4, 710–711. [PubMed: 19898521]

[16]. Imashiro C, Takeshita H, Morikura T, Miyata S, Takemura K, Komotori J, Sci. Rep. 2021, 11, 21466. [PubMed: 34728686]

[17]. Ghahremani FH, Sazgarnia A, Bahreyni-Toosi MH, Rajabi O, Aledavood A, Int. J. Hyperthermia 2011, 27, 625–636. [PubMed: 21846198]

[18]. Shchors K, Evan G, Cancer Res. 2007, 67, 7059–7061. [PubMed: 17671171]

[19]. Mallory M, Gogineni E, Jones GC, Greer L, Simone CB II, Crit. Rev. Oncol. Hematol. 2016, 97, 56–64. [PubMed: 26315383]

[20]. Wang Z, Li S, Zhang M, Ma Y, Liu Y, Gao W, Zhang J, Gu Y, Adv. Sci. 2017, 4, 1600327.

[21]. Pu Y, Wu W, Zhou B, Xiang H, Yu J, Yin H, Zhang Y, Du D, Chen Y, Xu H, Nano Today 2022, 44, 101461.

[22]. Li Y, Zhang K, Wu Y, Yue Y, Cheng K, Feng Q, Ma X, Liang J, Ma N, Liu G, Small 2022, 18, 2107461.

[23]. Peng J, Xiao Y, Li W, Yang Q, Tan L, Jia Y, Qu Y, Qian Z, Adv. Sci. 2018, 5, 1700891.

[24]. Wang M, Chang M, Zheng P, Sun Q, Wang G, Lin J, Li C, Adv. Sci. 2022, 9, 2202332.

[25]. Xie L, Li J, Wang G, Sang W, Xu M, Li W, Yan J, Li B, Zhang Z, Zhao Q, J. Am. Chem. Soc. 2022, 144, 787–797. [PubMed: 34985903]

[26]. Huang L, Li Y, Du Y, Zhang Y, Wang X, Ding Y, Yang X, Meng F, Tu J, Luo L, Sun C, Nat. Commun. 2019, 10, 4871. [PubMed: 31653838]

[27]. Mace TA, Zhong LW, Kokolus KM, Repasky EA, Int. J. Hyperthermia 2012, 28, 9–18. [PubMed: 22235780]

[28]. Chang M, Hou Z, Wang M, Li C, Lin J, Adv. Mater. 2021, 33, 2004788.

[29]. Bakker A, Kolff MW, Holman R, van Leeuwen CM, Straten L. K.-v., de Kroon-Oldenhof R, Rasch CRN, van Tienhoven G, Crezee H, Int. J. Radiat. Oncol. Biol. Phys. 2017, 98, 392–399. [PubMed: 28463159]

[30]. Ahmed K, Zaidi SF, Mati ur R, Rehman R, Kondo T, J. Therm. Biol. 2020, 91, 102615. [PubMed: 32716865]

[31]. Lepock JR, Int. J. Hyperthermia 2004, 20, 115–130. [PubMed: 15195506]

[32]. Lepock JR, Int. J. Hyperthermia 2003, 19, 252–266. [PubMed: 12745971]

[33]. Kaur P, Aliru ML, Chadha AS, Asea A, Krishnan S, Int. J. Hyperthermia 2016, 32, 76–88. [PubMed: 26757879]

[34]. Elming PB, Sorensen BS, Oei AL, Franken NAP, Crezee J, Overgaard J, Horsman MR, Cancers (Basel) 2019, 11, 60. [PubMed: 30634444]

[35]. Nikfarjam M, Muralidharan V, Christophi C, J. Surg. Res. 2005, 127, 208–223. [PubMed: 16083756]

[36]. Chu KF, Dupuy DE, Nat. Rev. Cancer 2014, 14, 199–208. [PubMed: 24561446]

[37]. Jacques SL, Phys. Med. Biol. 2013, 58, 5007–5008.

[38]. Johnson CC, Guy AW, Proc. IEEE 1972, 60, 692–718.

[39]. Finlayson L, Barnard IRM, McMillan L, Ibbotson SH, Brown CTA, Eadie E, Wood K, Photochem. Photobiol. 2022, 98, 974–981. [PubMed: 34699624]

[40]. Meinhardt M, Krebs R, Anders A, Heinrich U, Tronnier H, J. Biomed. Opt. 2008, 13, 044030. [PubMed: 19021357]

[41]. Bashkatov AN, Genina EA, Kochubey VI, Tuchin VV, J. Phys. D: Appl. Phys. 2005, 38, 2543–2555.

[42]. Dean-Ben XL, Gottschalk S, Mc Larney B, Shoham S, Razansky D, Chem. Soc. Rev. 2017, 46, 2158–2198. [PubMed: 28276544]

[43]. Abrams HL, Abrams' angiography: interventional radiology, Lippincott Williams & Wilkins, 2006.

[44]. Xu C, Pu K, Chem. Soc. Rev. 2021 50, 1111–1137. [PubMed: 33245316]

[45]. Xu C, Jiang Y, Huang J, Huang J, Pu K, Adv Mater. 2021, 33, e2101410. [PubMed: 34296785]

[46]. Jiang Y, Huang J, Xu C, Pu K, Nat Commun. 2021, 12, 742. [PubMed: 33531498]

[47]. Segelstein DJ, University of Missouri, Kansas City 1981.

[48]. Jaque D, Maestro LM, del Rosal B, Haro-Gonzalez P, Benayas A, Plaza JL, Rodriguez EM, Sole JG, Nanoscale 2014, 6, 9494–9530. [PubMed: 25030381]

[49]. Chen JY, Wiley B, Li ZY, Campbell D, Saeki F, Cang H, Au L, Lee J, Li XD, Xia YN, Adv. Mater. 2005, 17, 2255–2261.

[50]. Abadeer NS, Murphy CJ, J. Phys. Chem. C 2016, 120, 4691–4716.

[51]. Chen HJ, Shao L, Ming TA, Sun ZH, Zhao CM, Yang BC, Wang JF, Small 2010, 6, 2272–2280. [PubMed: 20827680]

[52]. Jiang K, Smith DA, Pinchuk A, J. Phys. Chem. C 2013, 117, 27073–27080.

[53]. Cho EC, Kim C, Zhou F, Cobley CM, Song KH, Chen J, Li Z-Y, Wang LV, Xia Y, J. Phys. Chem. C 2009, 113, 9023–9028.

[54]. Zeng J, Goldfeld D, Xia Y, Angew. Chem. Int. Ed. 2013, 52, 4169–4173.

[55]. Maestro LM, Haro-Gonzalez P, Sanchez-Iglesias A, Liz-Marzan LM, Sole JG, Jaque D, Langmuir 2014, 30, 1650–1658. [PubMed: 24495155]

[56]. Hessel CM, Pattani VP, Rasch M, Panthani MG, Koo B, Tunnell JW, Korgel BA, Nano Lett. 2011, 11, 2560–2566. [PubMed: 21553924]

[57]. Wang YC, Black KCL, Luehmann H, Li WY, Zhang Y, Cai X, Wan DH, Liu SY, Li M, Kim P, Li ZY, Wang LHV, Liu YJ, Xia YA, ACS Nano 2013, 7, 2068–2077. [PubMed: 23383982]

[58]. Xiao J-W, Fan S-X, Wang F, Sun L-D, Zheng X-Y, Yan C-H, Nanoscale 2014, 6, 4345–4351. [PubMed: 24622916]

[59]. Fu GL, Liu W, Feng SS, Yue XL, Chem. Commun. 2012, 48, 11567–11569.

[60]. Zha ZB, Deng ZJ, Li YY, Li CH, Wang JR, Wang SM, Qu EZ, Dai ZF, Nanoscale 2013, 5, 4462–4467. [PubMed: 23584573]

[61]. Zhou J, Lu ZG, Zhu XJ, Wang XJ, Liao Y, Ma ZF, Li FY, Biomaterials 2013, 34, 9584–9592. [PubMed: 24044996]

[62]. Zhou B, Li Y, Niu G, Lan M, Jia Q, Liang Q, ACS Appl. Mater. Inter. 2016, 8, 29899–29905.

[63]. Zhang X, Xu X, Li T, Lin M, Lin X, Zhang H, Sun H, Yang B, ACS Appl. Mater. Inter. 2014, 6, 14552–14561.

[64]. Lovell JF, Jin CS, Huynh E, Jin HL, Kim C, Rubinstein JL, Chan WCW, Cao WG, Wang LV, Zheng G, Nat. Mater. 2011, 10, 324–332. [PubMed: 21423187]

[65]. Yuan BH, Chen NG, Zhu Q, J. Biomed. Opt. 2004, 9, 497–503. [PubMed: 15189087]

[66]. Yamaoka Y, Harada Y, Nishino S, Maehara S, Hamano S, Takamatsu T, Proc. SPIE 2014, 8943, 89433C.

[67]. Jia P, Ji H, Liu S, Zhang R, He F, Zhong L, Yang P, J. Mater. Chem. B 2021, 9, 101–111. [PubMed: 33232438]

[68]. Atta S, Vo-Dinh T, ACS Appl. Nano Mater. 2022, 12562–12570. [PubMed: 36185168]

[69]. Skrabalak SE, Au L, Li XD, Xia YN, Nat. Protoc. 2007, 2, 2182–2190. [PubMed: 17853874]

[70]. Khlebtsov BN, Khanadeev VA, Burov AM, Le Ru EC, Khlebtsov NG, J. Phys. Chem. C 2020, 124, 10647–10658.

[71]. Liu X-L, Wang J-H, Liang S, Yang D-J, Nan F, Ding S-J, Zhou L, Hao Z-H, Wang Q-Q, J. Phys. Chem. C 2014, 118, 9659–9664.

[72]. Erkens M, Levshov D, Wenseleers W, Li H, Flavel BS, Fagan JA, Popov VN, Avramenko M, Forel S, Flahaut E, Cambre S, ACS Nano 2022, 16, 16038–16053. [PubMed: 36167339]

[73]. Wang F, Dukovic G, Brus LE, Heinz TF, Science 2005, 308, 838–841. [PubMed: 15879212]

[74]. Wei X, Li S, Wang W, Zhang X, Zhou W, Xie S, Liu H, Adv. Sci. 2022, 9, 2200054.

[75]. Maestro LM, Haro-González P, Del Rosal B, Ramiro J, Caamano A, Carrasco E, Juarranz A, Sanz-Rodríguez F, Solé JG, Jaque D, Nanoscale 2013, 5, 7882–7889. [PubMed: 23852326]

[76]. Curcio A, Van de Walle A, Benassai E, Serrano A, Luciani N, Menguy N, Manshian BB, Sargsian A, Soenen S, Espinosa A, Abou-Hassan A, Wilhelm C, ACS Nano 2021, 15, 9782–9795. [PubMed: 34032115]

[77]. Cheng X, Wang L, Xie L, Sun C, Zhao W, Liu X, Zhuang Z, Liu S, Zhao Q, Chem. Eng. J. 2022, 439, 135757.

[78]. BajalovicMeivita MP, LokeChan SSY, Go SX, Lee D, Bajalovic N, Loke DK, Acs Omega 2022, 7, 23075–23082. [PubMed: 35847245]

[79]. Guo LR, Panderi I, Yan DD, Szulak K, Li YJ, Chen YT, Ma H, Niesen DB, Seeram N, Ahmed A, Yan BF, Pantazatos D, Lu W, ACS Nano 2013, 7, 8780–8793. [PubMed: 24053214]

[80]. Li J-W, Zhou Y, Xu J, Gao F, Si Q-K, Wang J-Y, Zhang F, Wang L-P, ACS Appl. Mater. Inter. 2022, 14, 52670–52683.

[81]. Xu M, Zhao D, Chen Y, Chen C, Zhang L, Sun L, Chen J, Tang Q, Sun S, Ma C, Liang X, Wang S, ACS Appl. Mater. Inter. 2022, 14, 14072–14086.

[82]. Liao J-Z, Jiang Y, He F-F, Jiang L-L, Zhu X-M, Ke H, Mater. Today Chem. 2023, 27, 101324.

[83]. Liu C, Zhang S, Li J, Wei J, Muellen K, Yin M, Angew. Chem. Int. Ed. 2019, 58, 1638–1642.

[84]. Zhu K, Qian S, Guo H, Wang Q, Chu X, Wang X, Lu S, Peng Y, Guo Y, Zhu Z, Qin T, Liu B, Yang Y-W, Wang B, ACS Nano 2022, 11136–11151. [PubMed: 35749223]

[85]. Xu LG, Cheng L, Wang C, Peng R, Liu Z, Polym. Chem. 2014, 5, 1573–1580.

[86]. Sun X, Wang Y, Du T, Zhang Q, Li S, Chen Q, Wang M, Wang X, Ren L, Zhao X, Chin. Chem. Lett. 2023, 34.

[87]. Yang L, Guo H, Hou T, An B, Li F, Chin. Chem. Lett. 2023, 34, 107607.

[88]. Yu Z, Meng X, Zhang S, Wang X, Chen Y, Min P, Zhang Z, Zhang Y, Biomater. Sci. 2021, 10, 158–166. [PubMed: 34812815]

[89]. Li J, Yang M, Sun X, Yang X, Xue J, Zhu C, Liu H, Xia Y, Angew. Chem. Int. Ed. 2016, 128, 14032–14036.

[90]. Wang S, Huang P, Nie L, Xing R, Liu D, Wang Z, Lin J, Chen S, Niu G, Lu G, Adv. Mater. 2013, 25, 3055–3061. [PubMed: 23404693]

[91]. Chen Y-S, Zhao Y, Yoon SJ, Gambhir SS, Emelianov S, Nat. Nanotechnol. 2019, 14, 465–472. [PubMed: 30833692]

[92]. Yavuz MS, Cheng YY, Chen JY, Cobley CM, Zhang Q, Rycenga M, Xie JW, Kim C, Song KH, Schwartz AG, Wang LHV, Xia YN, Nat. Mater. 2009, 8, 935–939. [PubMed: 19881498]

[93]. Link S, Burda C, Mohamed MB, Nikoobakht B, El-Sayed MA, J. Phys. Chem. A 1999, 103, 1165–1170.

[94]. Prevo BG, Esakoff SA, Mikhailovsky A, Zasadzinski JA, Small 2008, 4, 1183–1195. [PubMed: 18623295]

[95]. Chen Y-S, Frey W, Kim S, Homan K, Kruizinga P, Sokolov K, Emelianov S, Opt. Express 2010, 18, 8867–8878. [PubMed: 20588732]

[96]. Moon H, Kumar D, Kim H, Sim C, Chang J-H, Kim J-M, Kim H, Lim D-K, ACS Nano 2015, 9, 2711–2719. [PubMed: 25751167]

[97]. Zha ZB, Yue XL, Ren QS, Dai ZF, Adv. Mater. 2013, 25, 777–782. [PubMed: 23143782]

[98]. MacDonald TD, Liu TW, Zheng G, Angew. Chem. Int. Ed. 2014, 53, 6956–6959.

[99]. Yang L, Huang B, Chen F, Jin J, Qin Z, Yang F, Li Y, Gu N, Langmuir 2020, 36, 12983–12989. [PubMed: 33085898]

[100]. Lu F, Li Z, Sheng Y, Ma Y, Yang Y, Ren Y, Su Z, Yu R, Zhang S, Biomaterials 2021, 276.

[101]. Liu Y, Bhattarai P, Dai Z, Chen X, Chem. Soc. Rev. 2019, 48, 2053–2108. [PubMed: 30259015]

[102]. Perrault SD, Walkey C, Jennings T, Fischer HC, Chan WCW, Nano Lett. 2009, 9, 1909–1915. [PubMed: 19344179]

[103]. Ernsting MJ, Murakami M, Roy A, Li S-D, J. Controlled Release 2013, 172, 782–794.

[104]. Marrache S, Pathak RK, Darley KL, Choi JH, Zaver D, Kolishetti N, Dhar S, Curr. Med. Chem. 2013, 20, 3500–3514. [PubMed: 23834187]

[105]. Kang H, Rho S, Stiles WR, Hu S, Baek Y, Hwang DW, Kashiwagi S, Kim MS, Choi HS, Adv. Healthc. Mater. 2020, 9, 1901223.

[106]. Li S-D, Huang L, Mol. Pharm. 2008, 5, 496–504. [PubMed: 18611037]

[107]. Guo XM, Wu Z, Li W, Wang ZH, Li QP, Kong FF, Zhang HB, Zhu XL, Du YPP, Jin Y, Du YZ, You J, ACS Appl. Mater. Inter. 2016, 8, 3092–3106.

[108]. Yang HY, Li Y, Lee DS, Macromol. Rapid Commun. 2020, 41, 2000106.

[109]. Barua S, Mitragotri S, Nano Today 2014, 9, 223–243. [PubMed: 25132862]

[110]. Rippe B, Haraldsson B, Physiol. Rev. 1994, 74, 163–219. [PubMed: 8295933]

[111]. Shi J, Kantoff PW, Wooster R, Farokhzad OC, Nat. Rev. Cancer 2017, 17, 20. [PubMed: 27834398]

[112]. West CML, Cooper RA, Loncaster JA, Wilks DP, Bromley M, Cancer Res. 2001, 61, 2907–2910. [PubMed: 11306466]

[113]. Chauhan VP, Stylianopoulos T, Martin JD, Popovic Z, Chen O, Kamoun WS, Bawendi MG, Fukumura D, Jain RK, Nat. Nanotechnol. 2012, 7, 383–388. [PubMed: 22484912]

[114]. Chen JY, Glaus C, Laforest R, Zhang Q, Yang MX, Gidding M, Welch MJ, Xia Y, Small 2010, 6, 811–817. [PubMed: 20225187]

[115]. Chithrani BD, Ghazani AA, Chan WCW, Nano Lett. 2006, 6, 662–668. [PubMed: 16608261]

[116]. He Y, Tian X, Fan X, Gong X, Tan S, Pan A, Liang S, Xu H, Zhou F, ACS Appl. Mater. Inter. 2023, 15, 552–565.

[117]. Zhao X, Yang X, Wang X, Zhao X, Zhang Y, Liu S, Anderson GJ, Kim S.-j., Li Y, Nie G, ACS Nano 2021, 15, 14149–14161. [PubMed: 34478262]

[118]. Cai Y, Ni D, Cheng W, Ji C, Wang Y, Muellen K, Su Z, Liu Y, Chen C, Yin M, Angew. Chem. Int. Ed. 2020, 59, 14014–14018.

[119]. Song C, Li Y, Li T, Yang Y, Huang Z, de la Fuente JM, Ni J, Cui D, Adv. Funct. Mater. 2020, 30, 1906309.

[120]. Zhang P, Chen D, Li L, Sun K, J. Nanobiotechnology 2022, 20, 1–27. [PubMed: 34980143]

[121]. Bie N, Yong T, Wei Z, Gan L, Yang X, Adv. Drug Del. Rev. 2022, 188, 114450.

[122]. Zhou WB, Liu XS, Ji J, J. Nanopart. Res. 2012, 14, 1128–1143.

[123]. Kobayashi S, Ohki A, Tanoue M, Inaoka Y, Murase K, Open J Appl. Sci. 2017, 7, 647–660.

[124]. Marches R, Mikoryak C, Wang RH, Pantano P, Draper RK, Vitetta ES, Nanotechnology 2011, 22, 095101. [PubMed: 21258147]

[125]. Baranov MV, Kumar M, Sacanna S, Thutupalli S, van den Bogaart G, Front. Immunol. 2021, 11, 3854.

[126]. Nomura T, Koreeda N, Yamashita F, Takakura Y, Hashida M, Pharm. Res. 1998, 15, 128–132. [PubMed: 9487559]

[127]. Huang J, Bu LH, Xie J, Chen K, Cheng Z, Li XG, Chen XY, ACS Nano 2010, 4, 7151–7160. [PubMed: 21043459]

[128]. Jiang W, Kim BYS, Rutka JT, Chan WCW, Nat. Nanotechnol. 2008, 3, 145–150. [PubMed: 18654486]

[129]. Wen W, Wu L, Chen Y, Qi X, Cao J, Zhang X, Ma W, Ge Y, Shen S, Drug Deliv J. Sci. Technol. 2020, 58, 101782.

[130]. Xu J, Song M, Fang Z, Zheng L, Huang X, Liu K, J. Controlled Release 2023, 353, 699–712.

[131]. Tian X, Ruan L, Zhou S, Wu L, Cao J, Qi X, Zhang X, Shen S, ACS Appl. Bio Mater. 2022, 5, 1692–1699.

[132]. Zeng X, Wang Y, Huang Y-S, Han J, Sun W, Butt H-J, Liang X-J, Wu S, Small 2022, 18, 2205461.

[133]. Zalba S, ten Hagen TLM, Burgui C, Garrido MJ, J. Controlled Release 2022, 351, 22–36.

[134]. Chang M, Hou Z, Wang M, Li C, Lin J, Adv. Mater. 2021, 33, 2004788.

[135]. Overchuk M, Weersink RA, Wilson BC, Zheng G, ACS Nano 2023, 17, 7979–8003. [PubMed: 37129253]

[136]. Bai Y, Yin J, Cheng J-X, Sci. Adv. 2021, 7, eabg1559. [PubMed: 33990332]

[137]. Das SS, Mahapatra SK, Comput. Methods Biomech. Biomed. Eng. 2023, 26, 721–733.

[138]. von Maltzahn G, Park J-H, Agrawal A, Bandaru NK, Das SK, Sailor MJ, Bhatia SN, Cancer Res. 2009, 69, 3892–3900. [PubMed: 19366797]

[139]. Ahuja AS, Prasad KN, Hendee WR, Carson PL, Med. Phys. 1978, 5, 418–421. [PubMed: 713975]

[140]. Duck FA, Physical properties of tissues: a comprehensive reference book, Academic press, 2013.

[141]. Cohen ML, J. Invest. Dermatol. 1977, 69, 333–338. [PubMed: 894075]

[142]. Choi J, Morrissey M, Bischof JC, J. Heat. Trans. T. Asme 2013, 135, 061302.

[143]. Chang M, Hou Z, Wang M, Wen D, Li C, Liu Y, Zhao Y, Lin J, Angew. Chem. Int. Ed. 2022, 61, e202209245.

[144]. Shende P, Bhandarkar S, Prabhakar B, Stem Cell Rev. Rep. 2019, 15, 637–651. [PubMed: 31254166]

[145]. Yun CW, Kim HJ, Lim JH, Lee SH, Cells 2020, 9, 60.

[146]. Albakova Z, Siam MKS, Sacitharan PK, Ziganshin RH, Ryazantsev DY, Sapozhnikov AM, Transl. Oncol. 2021, 14, 100995. [PubMed: 33338880]

[147]. Weng DS, Song BZ, Koido S, Calderwood SK, Gong JL, J. Immunol. 2013, 191, 755–763. [PubMed: 23772032]

[148]. Cheng J, Zhu Y, Dai Y, Li L, Zhang M, Jin D, Liu M, Yu J, Yu W, Su D, Zou J, Chen X, Liu Y, Angew. Chem. Int. Ed. 2023, e202304312.

[149]. Larson N, Gormley A, Frazier N, Ghandehari H, J. Controlled Release 2013, 170, 41–50.

[150]. Shen S, Feng L, Qi S, Cao J, Ge Y, Wu L, Wang S, Nano Lett. 2020, 20, 2137–2143. [PubMed: 32048853]

[151]. Wang J, Hao B, Xue K, Fu H, Xiao M, Zhang Y, Shi L, Zhu C, Adv. Mater. 2022, 34, 2205653.

[152]. Ng KK, Weersink RA, Lim L, Wilson BC, Zheng G, Angew. Chem. Int. Ed. 2016, 55, 10003–10007.

[153]. Weiss N, Sosna J, Goldberg SN, Azhari H, Int. J. Hyperthermia 2014, 30, 119–125. [PubMed: 24571175]

[154]. Guo G-P, Su H-D, Ding H-P, Ma Q-Y, Acta. Phys. Sin. 2017, 66, 164301.

[155]. Momenroodaki P, Haines W, Fromandi M, Popovic Z, IEEE Trans. Microwave Theory Tech. 2018, 66, 2535–2545.

[156]. Meng X, Zhang B, Yi Y, Cheng H, Wang B, Liu Y, Gong T, Yang W, Yao Y, Wang H, Bu W, Nano Lett. 2020, 20, 2522–2529. [PubMed: 32208714]

[157]. Zhen X, Xie C, Pu K, Angew. Chem. Int. Ed. 2018, 57, 3938–3942.

[158]. Kim J, Choi W, Park E-Y, Kang Y, Lee KJ, Kim HH, Kim WJ, Kim C, IEEE Trans. Biomed. Eng. 2019, 66, 3330–3338. [PubMed: 30869607]

[159]. Gellermann J, Wlodarczyk W, Hildebrandt B, Ganter H, Nicolau A, Rau B, Tilly W, Fahling H, Nadobny J, Felix R, Wust P, Cancer Res. 2005, 65, 5872–5880. [PubMed: 15994965]

[160]. Fried MP, Morrison PR, Hushek SG, Kernahan GA, Jolesz FA, Lasers Surg. Med. 1996, 18, 410–419. [PubMed: 8732581]

[161]. Bazrafshan B, Hubner F, Farshid P, Hammerstingl R, Paul J, Vogel V, Mantele W, Vogl TJ, Lasers Med. Sci. 2014, 29, 173–183. [PubMed: 23535892]

[162]. Quesson B, de Zwart JA, Moonen CTW, J. Magn. Reson. Imaging 2000, 12, 525–533. [PubMed: 11042633]

[163]. Odeen H, Parker DL, Prog. Nucl. Magn. Reson. Spectrosc. 2019, 110, 34–61. [PubMed: 30803693]

[164]. Lewis MA, Staruch RM, Chopra R, Int. J. Hyperthermia 2015, 31, 163–181. [PubMed: 25753369]

[165]. Arthur RM, Straube WL, Trobaugh JW, Moros EG, Int. J. Hyperthermia 2005, 21, 589–600. [PubMed: 16147442]

[166]. Kuroda K, Oshio K, Mulkern RV, Jolesz FA, Magn. Reson. Med. 1998, 40, 505–510. [PubMed: 9771566]

[167]. Amiri H, Makkiabadi B, Front. biomed. technol. 2020, 7, 82–91.

[168]. Fujiwara M, Sun S, Dohms A, Nishimura Y, Suto K, Takezawa Y, Oshimi K, Zhao L, Sadzak N, Umehara Y, Teki Y, Komatsu N, Benson O, Shikano Y, Kage-Nakadai E, Sci. Adv. 2020, 6, eaba9636. [PubMed: 32917703]

[169]. Zhu X, Feng W, Chang J, Tan Y-W, Li J, Chen M, Sun Y, Li F, Nat. Commun. 2016, 7, 10437. [PubMed: 26842674]

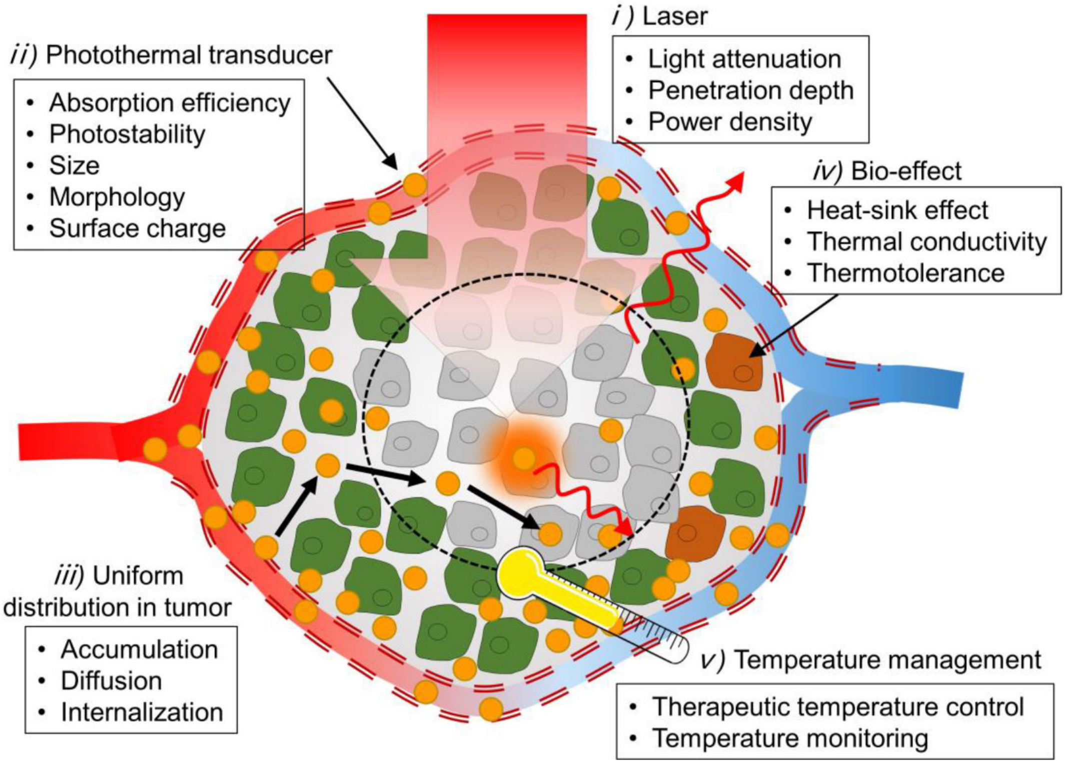

Figure 1.

Schematic illustration showing the parameters that affect the efficacy of PTT *in vivo*: i) the attenuation in tissue, penetration depth, and irradiance of the laser; *ii*) the absorption coefficient, photothermal conversion efficiency, photostability, particle size, shape, and surface property of the photothermal transducers; *iii*) the spatial distribution of the transducers; *iv*) the heat-sink effect, thermal conductivity, thermotolerance of the lesion; and *v*) the actual temperature involved in the therapy.

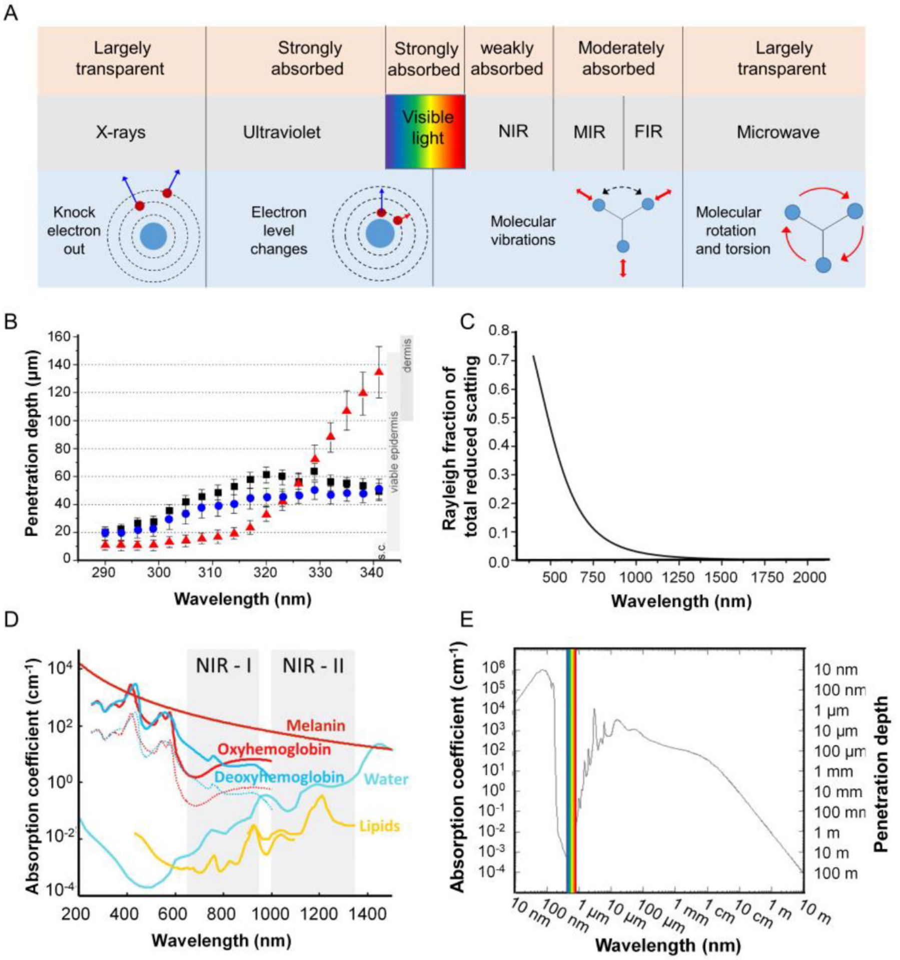

Figure 2.

(A) Schematic illustration of the tissue absorption of light with different wavelengths. (B) Penetration depths of UV radiation in human skin. The wavelength dependence of the penetration depth is similar at the volar (■) and dorsal (●) aspect of the forearm. Spectral characteristics are different at the thenar (▲). The penetration depth is only very slowly rising in the UVB and increases steeply in the UVA. Reproduced with permission.[40] Copyright 2008, SCImago. (C) Fraction of total reduced scattering attributed to Rayleigh scattering in skin. Reproduced with permission.[41] Copyright 2005, IOP science. (D) Optical absorption spectra of major endogenous chromophores at typical concentrations occurring in living mammalian tissues. The first (NIR-I) and second (NIR-II) windows, where optical absorption is minimized, are indicated. Reproduced with permission.[42] Copyright 2005, Royal Society of Chemistry. (E) Absorption spectrum of liquid water with the wavelength in the range of 10 nm and 10 m. Reproduced with permission.[47] Copyright 1981, University of Missouri.

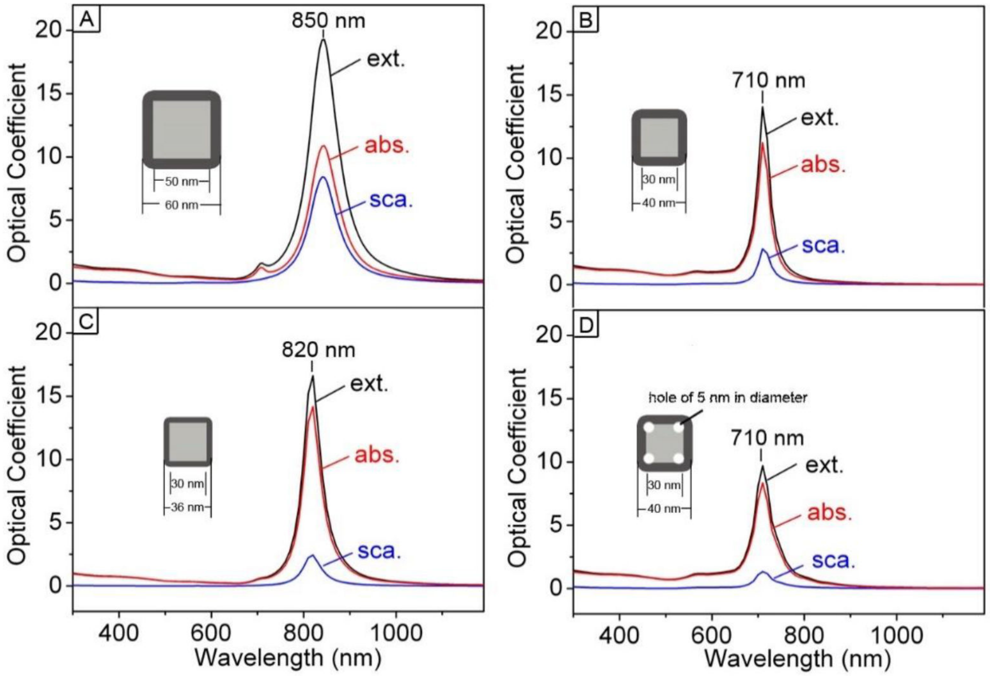

Figure 3.

Extinction, absorption, and scattering spectra calculated using the DDA method for a Au nanoparticle dispersed in water (n = 1.33): (A) a Au nanobox with an inner edge length of 50 nm and a wall thickness of 5 nm; (B) a Au nanobox with an inner edge length of 30 nm and a wall thickness of 5 nm; (C) a Au nanobox with an inner edge length of 30 nm and a wall thickness of 3 nm; and (D) an Au nanobox with an inner edge length of 30 nm and a wall thickness of 5 nm, together with holes of 5 nm in edge length in the corners. Reproduced with permission.[49] Copyright 2005, Wiley-VCH.

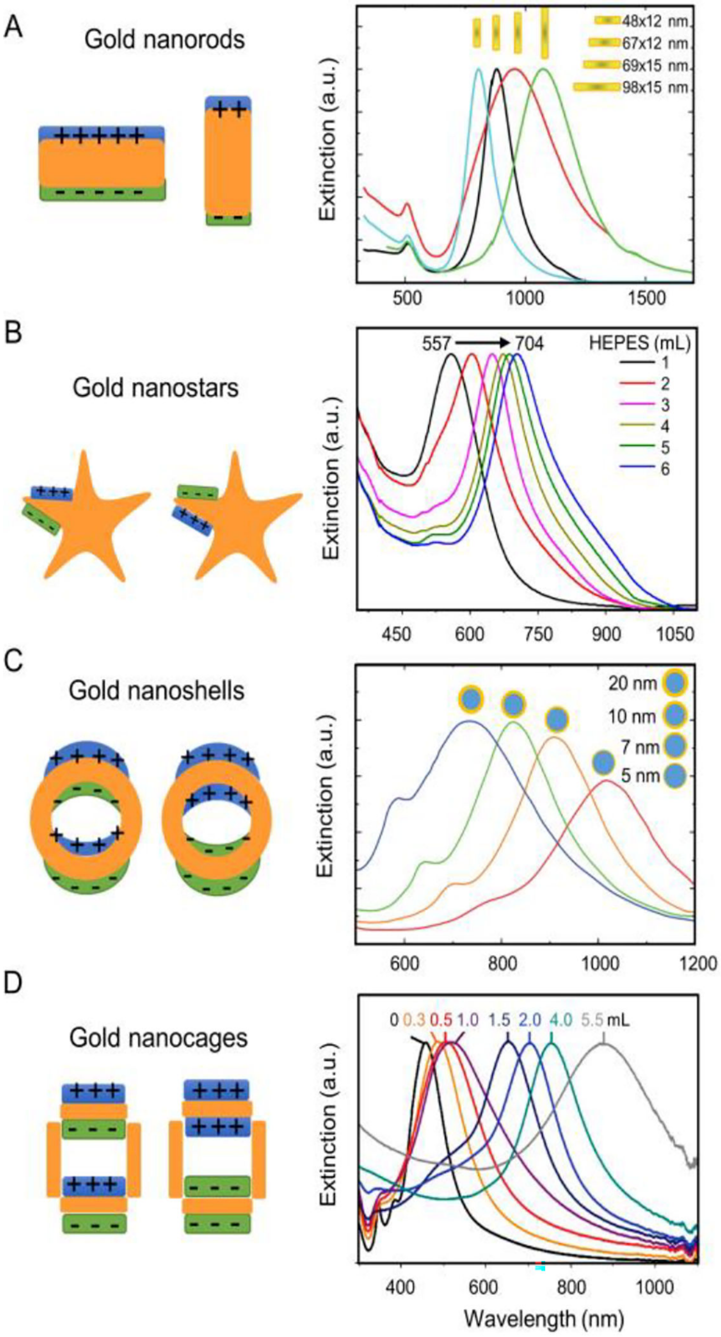

Figure 4.

Schematic showing the localized surface plasmon resonances and extinction spectra of (A) Au nanorods with different aspect ratios, (B) Au nanostars with different aspect ratios, (C) SiO_2@Au core-shell nanoshells with different shell thicknesses, and (D) Au nanocages with different wall thicknesses. (A) and (C) were reproduced with permission.[48] Copyright 2014, Royal Society of Chemistry. (B) Reproduced with permission.[71] Copyright 2014, American Chemistry Society. (D) Reproduced with permission.[64] Copyright 2011, Springer Nature.

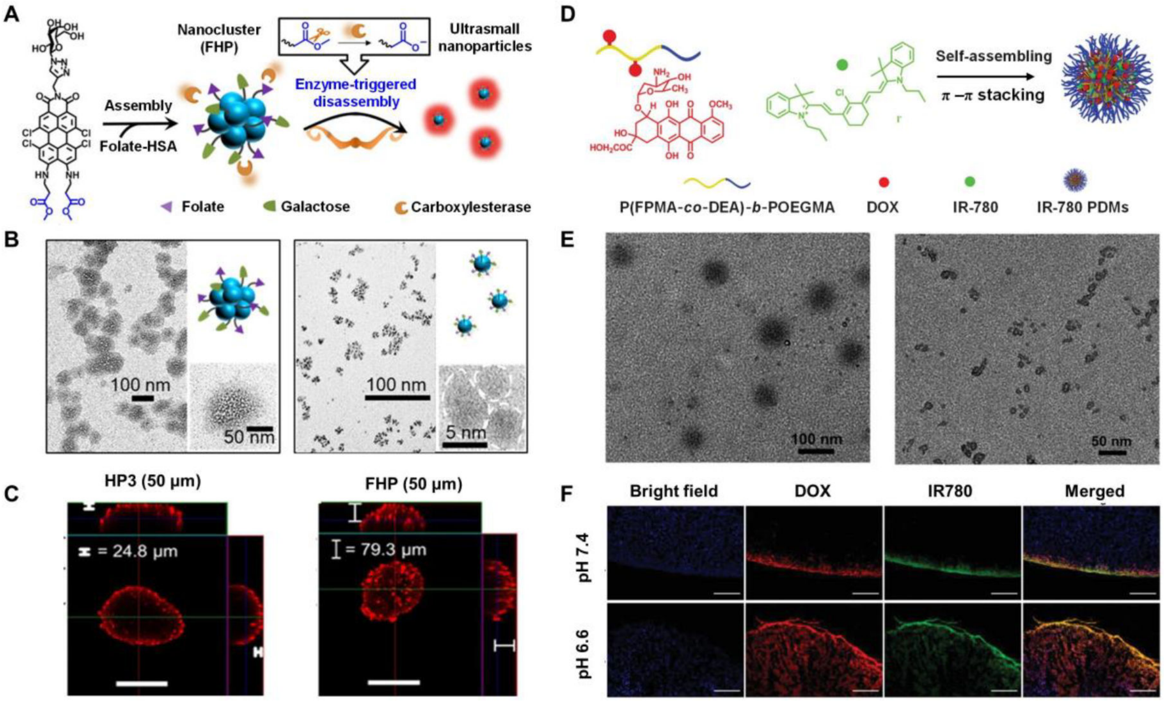

Figure 5.

(A) Schematic illustration of the aggregate formation and the carboxylesterase-triggered disassembly. (B) TEM images and schematic illustrations of the aggregates before (left) and after (right) the treatment with carboxylesterase. (C) Fluorescence images of the multicellular spheroids showing the penetration depth of carboxylesterase-responsive tetrachloroperylene monoimide-human serum albumins nanoclusters (FHP) and carboxylesterase-irresponsive nanoclusters (HP3) through orthogonal section view of x/z axes (top) and y/z axes (right). scale bar: 200 μm. (A-C) Reproduced with permission.[118] Copyright 2020, Wiley-VCH. (D) Schematic showing the formation of pH-sensitive doxorubicin and IR780 loaded poly(4-formylphenyl methacrylate-co-2-(diethylamino) ethyl methacrylate)-b-polyoligoethyleneglycol methacrylate (PDMs). (E) TEM image of PDMs at pH=7.4 (left) and pH=6.6 (right) showing the assembly and disassembly, respectively. (D-F) Reproduced with permission.[119] Copyright 2020, Wiley-VCH.

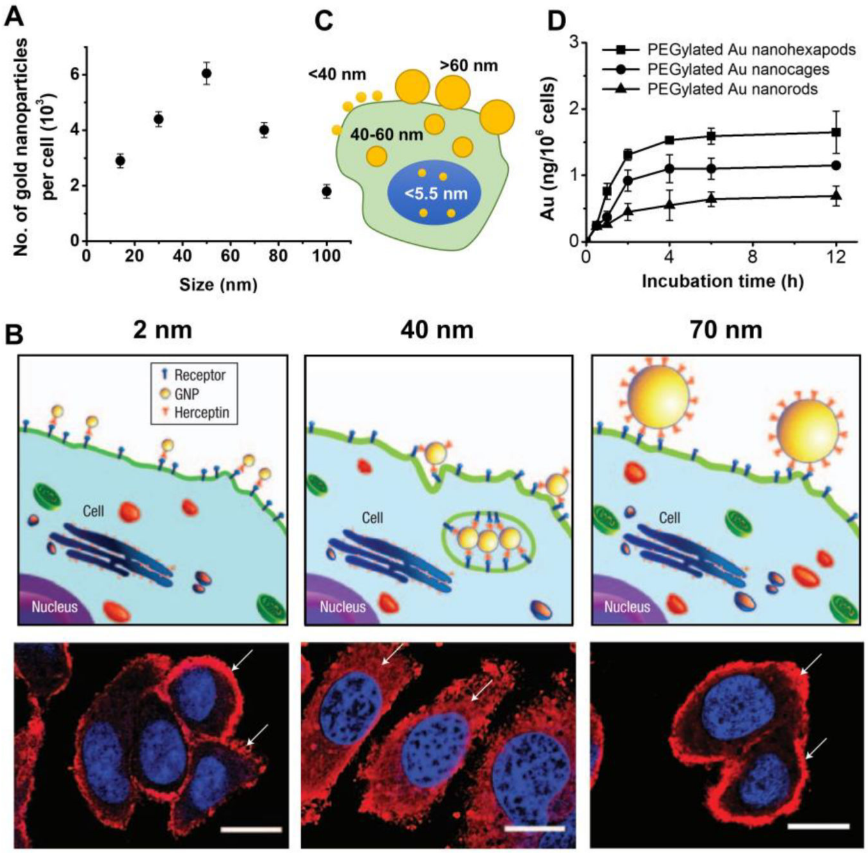

Figure 6.

(A) Cellular uptake of gold nanoparticles as a function of size. Reproduced with permission.[115] Copyright 2006, American Chemistry Society. (B) Herceptin-gold nanoparticles (Her-GNPs) with a size of 40 nm in diameter could down-regulate the membrane ErbB2 receptor (red) and redistribute the receptor from the cell surface to the cytoplasm, while 2 and 70 nm Her-GNPs did not show this effect. Scale bars: 10 μm. Reproduced with permission.[128] Copyright 2008, Springer Nature. (C) Schematic showing that nanoparticles with a size of 40–60 nm are more readily to be uptaken than those smaller than 40 nm or larger than 60 nm. Nanoparticles smaller than 5.5 nm can enter into the nucleus. (D) Uptake of the PEGylated gold nanohexapods, nanocages, and nanorods by MDA-MB-435 cells after incubation for different periods of time. The cells were positioned in an inverted configuration. The initial concentration of the gold nanoparticles in the culture medium were 10 μg/mL for all samples. Reproduced with permission.[57] Copyright 2013, American Chemistry Society.

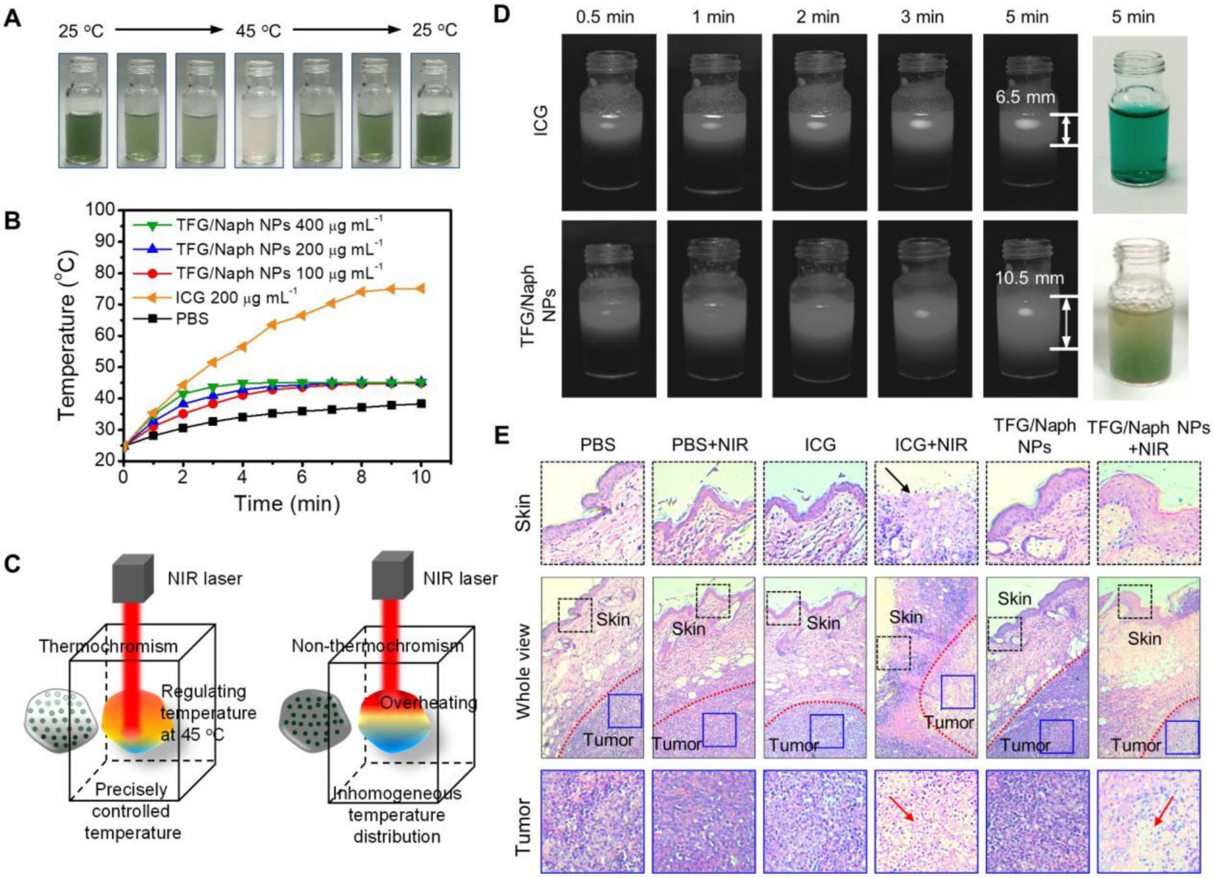

Figure 7.

A) Digital images showing the color changes of a suspension of the thermochromic nanoparticles when its temperature was raised from 25 to 45, and then decreased to 25 °C. B) Temperature profiles of ICG and (2′-phenylamino)-6′-diethylamino fluoran/β-naphthol (TFG/Naph) nanoparticles upon the irradiation of NIR light. C). Schematic illustration showing the thermostatic PTT in a tumor. D) Digital images showing the penetration depth of the light. E) The H&E staining sections of the tumor and adjacent tissues after PTT. Reprinted with permission.[150] Copyright 2020, American Chemistry Society.

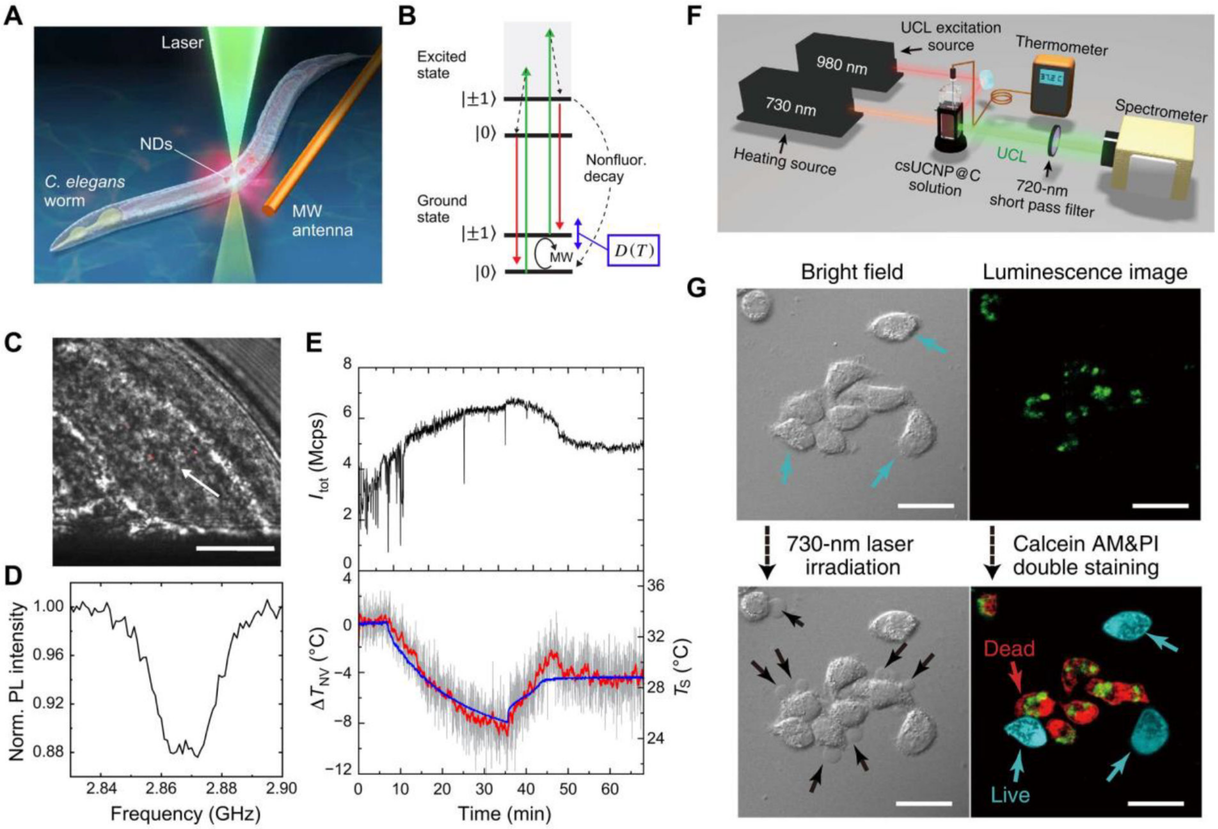

Figure 8.

A) Monitoring of temperature *in vivo* using a nanodiamond (ND) thermometer. B) A schematic illustration of the energy diagram of the nitrogen-vacancy centers. C) Microscopy image of the worm labelled with nanodiamonds. Scale bar: 20 μm. D) The fluorescence from nanodiamond at different continuous wave frequency. E) Time profiles of the total photon counts (I_{tot}) and the estimated temperature of the nanodiamonds. F) Schematic illustration of the setup for the detection of the eigen temperature of csUCNP@C. G) Cells with and without csUCNP@C were irradiated with 730-nm and 980-nm lasers, respectively. Scale bar: 30 mm. (A-E) Reprinted with permission.[168] Copyright 2020, American Association for the Advancement of Science. (F-G) Reprinted with permission.[169] Copyright 2016, Springer Nature.

Table 1.

Penetration depth of electromagnetic waves with different wavelengths in biological media.[38]

Frequency (MHz)	Wavelength (cm)	Depth of penetration (cm)	
		Muscle, skin, and tissues with high water content	Fat, bone, and tissues with low water content
1	30000	91.3	
10	3000	21.6	
27.12	1106	14.3	159
40.68	738	11.2	118
100	300	6.66	60.4
200	150	4.79	39.2
300	100	3.89	32.1
433	69.3	3.57	26.2
750	40	3.18	23
915	32.8	3.04	17.7
1500	20	2.42	13.9
2450	12.2	1.70	11.2
3000	10	1.61	9.74
5000	6	0.788	6.67
5800	5.17	0.720	5.24
8000	3.75	0.413	4.61
10000	3	0.343	3.39

Table 2.

Optical properties of different types of nanoscale transducers.

Nanoparticles	dimension (nm)	λ_{max} (nm)	Molar extinction coefficient ($M^{-1}cm^{-1}$)	Absorption efficiency	Ref.
Au nanorods	5 radius 27 length	808	1.9×10^9	0.96	[56]
Au nanocages	47 ± 3 nm edge 4 ± 1 wall thickness	808	1.3×10^{11}	0.63	[55]
Au nanoshells	55 radius 65 radius	800	2×10^{11}	0.61	[56]
Au nanohexapods	25.3 core radius 16.3 arm length 13.6 arm width	805	5.0×10^9	0.91	[57]
Pd	26.9±3.2 edge 22.8±2.5 nm	808	6.3×10^7	—	[58]
Carbon nanotubes	0.6 radius 150 length	808	7.9×10^6	0.5	[48, 56]
CuSe-QDs	8	970	7.7×10^7	0.22	[48, 56]
CdX (X = S, Se, Te)	2	—	$\sim2–5\times10^5$	0.14	[48, 56]
Prussian blue nanoparticles	42	808	1.09×10^9	—	[59]
PPy	46	808	2.4×10^{10}	—	[60]
PANi nanoparticles	48.5±1.5	808	8.95×10^8	0.49	[61]
RC-BSA	110	915	0.83×10^5	—	[62]
PPy-enveloped Fe_3O_4 NPs	100	808	1.12×10^9	—	[63]
Porphysomes	100	680	2.9×10^9	—	[64]
ICG	Molecular	780	$\sim4.5\times10^5$	—	[65]
IR 780	Molecular	780	2.8×10^5	—	[66]
IR 808	Molecular	808	3×10^5	—	[67]